Final version published in: Coordination Chemistry Reviews 352, 67-82, 2017.
https://doi.org/10.1016/j.ccr.2017.08.019

'Electronic Structure Elucidation in Oxidized Metal Salen Complexes'

Ryan M. Clarke[a], Khrystyna Herasymchuk[a], and Tim Storr[a*]

[a]Department of Chemistry, Simon Fraser University, 8888 University Drive, Burnaby, BC, Canada, V5A 1S6.

*tim_storr@sfu.ca

Keywords: electronic structure, salen, redox-active ligands, mixed-valence, intervalence charge transfer, biomimetic models

Abstract

Salen ligands are ubiquitous in inorganic chemistry with utility in applications ranging from materials to catalysis. Additionally, salen ligands have the potential for redox-activity due to energetically accessible molecular orbitals. This review will focus on elucidation of the electronic structure in oxidized metal salen complexes. Due to the highly modular synthesis of these ligands, we present a comprehensive examination of structural factors that play a role in determining the overall electronic structure upon one-electron oxidation. Experimental and theoretical techniques used in the study of oxidized metal-salen complexes are presented, as well as the basics for the interpretation of such techniques. While the emphasis of the review is on complexes of the first-row transition metals, we briefly discuss second- and third-row transition metal salen complexes, as well as salen-type ligand derivatives.

Final version published in: Coordination Chemistry Reviews 352, 67-82, 2017.
https://doi.org/10.1016/j.ccr.2017.08.019

1. Introduction

The study of transition metal complexes with pro-radical ligands is an area of considerable research interest due to the ability of these ligands to confer noble-metal reactivity to base metals [1-6]. The relative ordering of the metal and ligand frontier molecular orbitals in a transition metal complex ($M^{n+}L$) incorporating pro-radical ligands dictates whether oxidation/reduction occurs at the metal or the ligand (Eqn. 1).

$$[M^{n+1}L^{\bullet}]^{-} \text{ or } [M^{n-1}L]^{-} \xleftarrow{\text{Reduction}} M^{n+}L \xrightarrow{\text{Oxidation}} [M^{n+1}L]^{+} \text{ or } [M^{n+}L^{\bullet}]^{+}$$

Pro-radical ligands are essential in the active sites of many metalloenzymes as the coupling of redox events at both metal and ligand allows for efficient multielectron chemistry [7]. Examples include photosystem II [8,9], cyctochrome *c* oxidase [10] and P450 [11], glyoxal oxidase [12], and galactose oxidase (GOase) [13].

GOase is a copper containing metalloenzyme that catalyzes the oxidation of primary alcohols to aldehydes with the concomitant reduction of O_2 to H_2O_2 [14,15]. The active-site coordination sphere is composed of two equatorial histidine residues (His_{496} and His_{581}), a post-translationally modified tyrosine residue (Tyr_{272}) cross-linked with a cysteine residue (Cys_{228}) and an axial tyrosine residue (Tyr_{495}). Scheme 1 depicts the mechanistic steps involved in this transformation [14]. The catalytically active form, GO_{ox}, incorporates a Cu(II) metal centre and a tyrosyl ligand radical, with each undergoing one-electron reduction during substrate oxidation [13].

Final version published in: Coordination Chemistry Reviews 352, 67-82, 2017.
https://doi.org/10.1016/j.ccr.2017.08.019

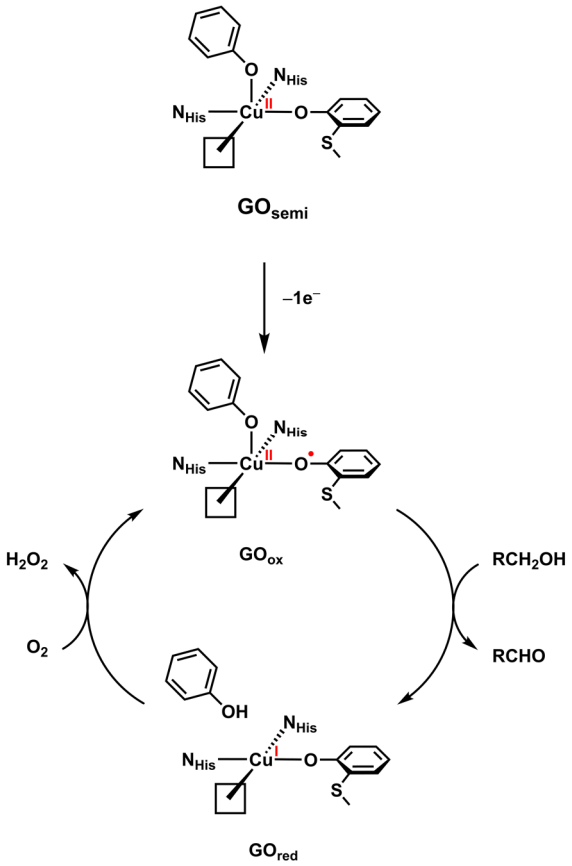

Scheme 1. Mechanism of the aerobic oxidation of primary alcohols to aldehydes catalyzed by galactose oxidase (GO_{ase}).

Owing to the simplicity of the active site in GO_{ase} and other metalloenzymes, many structural and functional small-molecule models of these enzymes have been studied [16-21]. In particular the electronic structures of one-electron oxidized metal complexes of phenolate containing ligands such as salen (salen is a common abbreviation for N_2O_2 bis-Schiff-base bis-phenolate ligands) have been extensively utilized due to their modular syntheses allowing for facile tuning of both steric and electronic properties, versatility in catalysis and structural similarity (N and O donor moieties) to biological coordination spheres [22-27]. Furthermore, salen ligands are known to coordinate to a wide variety of transition and main group metal centres in a number of oxidation states [28]. Traditionally, the term salen (Sal) refers to ligands specifically prepared *via*

Final version published in: Coordination Chemistry Reviews 352, 67-82, 2017.
https://doi.org/10.1016/j.ccr.2017.08.019

condensation of two equivalents of salicylaldehyde and ethylenediamine, but has come to include ligands with varying phenyl ring substituents and diamine backbones [29] (Fig. 1). The imine functionalities can be reduced to afford the corresponding tetrahydrosalen analogues [30-33], while half-reduced salen ligands can be prepared *via* reduction of only one imine function [27]. The development of synthetic methodologies for asymmetric salens (ligands with different substitution patterns on each of the phenol moieties) allows for the preparation of a diverse library of ligands [34].

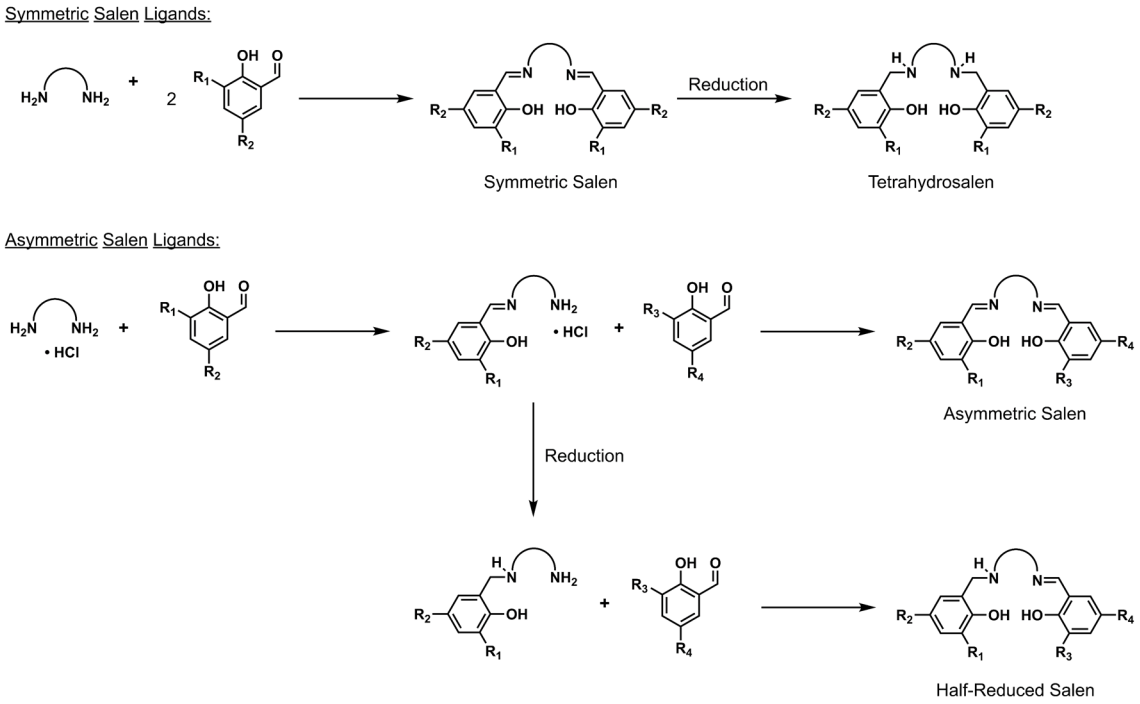

Figure 1. Synthetic strategies for symmetric and asymmetric salen ligands.

Metal-salen complexes can exhibit redox activity at either the ligand or the metal centre upon one-electron oxidation, depending on the transition metal used, the peripheral ligand substituents, the solvent or the temperature. Without the use of *ortho*- and *para*-phenolate protecting groups to

prevent radical coupling, oxidized metal salen complexes can be prone to rapid polymerization, restricting the study of oxidized species [35-39].

Metal-salen ligand radical complexes are amongst a class of compounds known as mixed-valence compounds, which traditionally consist of two metal ions in different formal oxidation states bridged by an organic linker (M^{n+}–L–M^{n+1}) [40,41]. The archetypical example of a mixed valence compound of this type is the Creutz-Taube ion, a diruthenium complex bridged by a pyrazine ligand with the formula $[((NH_3)_5Ru)(\mu\text{-pyz})(Ru(NH_3)_5)]^{5+}$ [42]. The mixed-valency is inverted in the case of metal-salen ligand-radical complexes, in which two redox active phenolates are bridged by a transition metal centre (L–M^{n+}–L$^{\bullet}$) [43,44]. Robin and Day established a classification system for the characterization of mixed-valence compounds depending on the degree of electronic communication between the valencies [45], and Hush provided a theoretical model to describe the intervalence charge transfer (IVCT) [46]. Class I mixed-valence compounds are those that are unable to undergo intramolecular electron transfer from one valence site to another due to distance between the valence sites, or limited coupling through the spacer group. Class II mixed-valence complexes are those in which the valences can interconvert under thermal or photochemical activation, while Class III mixed-valence compounds are coupled so strongly that delocalization occurs and the formal charge on each valence is averaged. The Creutz-Taube ion is an example of a Class III mixed-valence compound in which the Ru centres are best described as $Ru^{2.5+}$-L-$Ru^{2.5+}$ [41,47]. Class II and III systems exhibit IVCT bands in the NIR region of their absorption spectra, and thus information pertaining to the degree of delocalization in these systems can be easily extracted [48,49]. Class II mixed-valence species are characterized by broad, relatively weak and solvent dependent IVCT bands, whereas compounds belonging to Class III are characterized by sharp, intense and

solvent independent IVCT bands (Table 1). It is important to note that while Class III complexes are said to display IVCT transitions, the transitions do not involve net transfer of charge from one valence to the other, but instead the IVCT transition occurs within the molecular orbital manifold of the system. As a consequence of the sensitivity of the IVCT bands to localization / delocalization, and the significant theory developed to account for these bands, UV-vis-NIR spectroscopy is routinely employed in the study of one-electron oxidized metal-salen complexes to deduce the degree of localization/delocalization of the resultant electron hole [41,50-52].

Table 1. Optical properties of IVCT bands in mixed valence compounds.

	$\Delta\nu_{1/2}$	ε_{max}
Class I	No coupling	
Class II	$\geq$ 2,000 cm^{-1}	$\leq$ 5,000 M^{-1} cm^{-1} (solvent dependent)
Class III	$\leq$ 2,000 cm^{-1}	$\geq$ 5,000 M^{-1} cm^{-1} (solvent independent)

While UV-vis-NIR spectroscopy is an invaluable tool for determining the extent to which the electron hole is delocalized, other experimental and theoretical techniques are routinely employed (Table 2). Electrochemical analysis is often the first technique investigated as it provides the oxidation potential of the system under study. This allows for the careful selection of an appropriate chemical oxidant [53] or the potential for electrochemical oxidation. Information pertaining to delocalization can also be determined from electrochemical measurements, as two uncoupled phenolate rings (Class I) will undergo oxidation at approximately the same potential (effectively doubling the observed current) [54]; any electronic interaction between the two rings however (Class II or Class III) will manifest as a larger separation of oxidation events for each phenolate ring [55-57]. Electrochemical data can be

misleading however, due to the significant dependence of redox potentials on solvent, as well as the electrolyte [51]. Metal or ligand based oxidation can be distinguished using electron paramagnetic resonance (EPR) spectroscopy. Ligand-based radicals will exhibit *g* values close to the free electron value (g_e = 2.002319). Furthermore, the observed *g* value is sensitive to metal ion participation to the singly occupied molecular orbital (SOMO) [58,59]. In some cases, hyperfine coupling to spin-active nuclei is resolvable, for example 3 or 5 line patterns in the g_{zz} component of pyridine adducts of Ni salen complexes arising from hyperfine coupling to one or two axially bound N_{pyr} atoms (S_N = 1). Resonance Raman (rR) spectroscopy is a useful tool for assigning an oxidized salen complex as Class II or Class III. Class II complexes exhibit vibrational modes resonant with both phenoxyl $\pi \rightarrow \pi^*$ and phenolate → Ni(II) LMCT transitions, whereas only modes resonant with phenoxyl $\pi \rightarrow \pi^*$ transitions are observed for a fully delocalized Class III system [60-63]. In cases where X-ray quality crystals of oxidized products are obtained, solid-state metrical parameters can provide insight into the locus of oxidation and degree of delocalization. For example, a symmetric distribution of metrical parameters suggests either a fully delocalized electronic structure or metal based oxidation, whereas an asymmetric distribution, with one side of the salen ligand exhibiting a quinoidal distribution of bond lengths, and the other aromatic, is suggestive of a localized electronic structure [64]. X-ray absorption spectroscopy (XAS) can be used to probe the metal oxidation state, as well as nearest neighbour distances, in the solid state or frozen solution. For example, in Cu salen complexes, the Cu K-edge 1s → 3d transition is a sensitive indicator of copper oxidation state [65] and a shift to higher energy can be attributed to an increase in metal oxidation state. Additionally, nearest neighbour distances can be obtained, but extracting bond length changes upon oxidation can be complicated for salens due to an inability to discriminate

between N and O atoms in the backscattering data. Finally, theoretical calculations (such as density functional theory – DFT) are very useful in further understanding electronic structure, including the electronic groundstate, visualization of the singly occupied molecular orbital and spin density, as well the predicted donor and acceptor orbitals associated with the IVCT transition (*via* time-dependent density functional theory – TD-DFT). There is a tendency for DFT calculations to favor more symmetrically delocalized structures [58,66], and thus one must be cautious in interpreting DFT results and consider benchmarking against experimental data.

Table 2. Experimental and theoretical techniques commonly used in studying oxidized metal salen complexes.

Technique	Readout
UV-vis-NIR spectroscopy	Energy, shape, and intensity of NIR bands provide insight into the electronic structure and degree of radical delocalization.
Electrochemistry	Accessibility and reversibility of redox processes, stability of oxidized forms, coupling between redox-active moieties.
Electron paramagnetic resonance (EPR)	Locus of oxidation. Interaction of unpaired electron with spin-active nuclei. Ligand-based oxidation results in *g* values close to the free electron value (g_e = 2.002319), with any deviation associated with metal-character in the SOMO.

Resonance Raman (rR)	Vibrational modes associated with the phenoxyl and phenolate ligand redox states. Radical localization results in the appearance of both phenoxyl and phenolate bands.
X-Ray crystallography	Ligand and coordination sphere bond length changes that can be assigned to localization / delocalization of the ligand radical, or metal based oxidation.
X-ray absorption spectroscopy (XAS)	Metal oxidation state and nearest neighbour distances in the solid state or frozen solution.
Magnetic susceptibility	Solid-state and solution (^{1}H NMR Evans' method) measurements to assign ground-state electronic structure [67,68].
Theoretical calculations	Prediction of electronic groundstate, visualization of SOMO, spin density, and donor/acceptor orbitals associated with NIR bands.

In this review, we survey recent progress in the characterization of the electronic structure of oxidized metal salen complexes. It is our goal to familiarize the reader with the critical factors that lead to localization or delocalization upon one electron oxidation, and how this relates to subsequent reactivity. We have organized this review into sections by metal ion, and while much of the work in this field has focused on complexes of the first row, we will also briefly discuss

chemistry of heavier metals, as well as related systems such as anilinosalen and phosphosalen analogues.

2. Manganese

Manganese salen complexes are among the most extensively studied of this class due to their utility as catalysts in the Jacobsen-Katsuki epoxidation reaction [22,28,69-72]. While thoroughly investigated in the context of epoxidation, manganese salen complexes also find applicability both stoichiometrically and catalytically in important reactions such as benzylic C-H fluorination [73] and nitrene transfer to electron-rich olefins [74-76]. Manganese salen complexes also find utility as starting materials in the preparation of other transition metal nitride complexes [77-79]. A number of reports investigate differential activity as a consequence of altered chemical structure [80-85], however few describe the resultant electronic structure upon metal complex oxidation. One of the first such reports by Fujii and co-workers aimed to establish structural and reactivity differences between Mn(IV)-phenolate and Mn(III)-phenoxyl-radical electronic structures as potential intermediates involved in the Jacobsen-Katsuki epoxidation reaction; while also establishing key spectroscopic signatures for these two distinct electronic structures employing UV-Vis-NIR, EPR and resonance Raman spectroscopies [86] (Fig. 2).

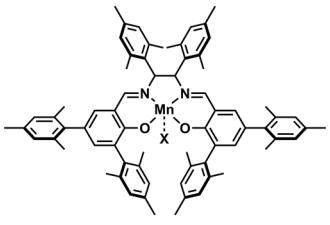

X = OH_2 (**1**), OH (**2**), =O (**3**)

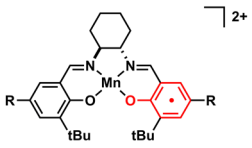

R = OMe (**4**), tBu (**5**), Ph (**6**)

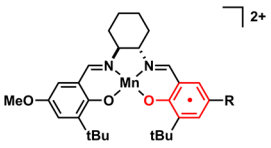

R = tBu (**7**), Cl (**8**)

Figure 2. Mn salen complexes studied by Fujii and co-workers including both symmetric and asymmetric structures.

Of the oxidized intermediates investigated, only [**1**]$^+$ was assigned as a Mn(III)-phenoxyl radical after one-electron oxidation, while both [**2**]$^+$ and [**3**]$^+$ are better formulated as Mn(IV)-phenolate electronic structures. Structurally, complexes [**1**-**3**] differ only in their degree of protonation, however, there is a clear reactivity difference as a consequence of a change in electronic structure from Mn(III)-phenoxyl radical to Mn(IV)-phenolate. Only [**3**]$^+$ is capable of appreciably transferring its oxygen atom or undergoing hydrogen atom abstraction reactions, while [**2**] shows significantly reduced oxidizing activity. [**1**]$^+$ is readily converted to [**2**]$^+$ by the addition of Bu_4NOH, which cannot be converted back to [**1**]$^+$ even with the addition of a strong protic acid CF_3SO_3H. This suggests that the formation of the inactive Mn(III)-phenoxyl radical electronic structure is energetically unfavourable under the conditions investigated. Furthermore, this suggests that the redox potential of the Mn(III) ion and the salen phenolate are very close, which warrants careful investigation of the locus of oxidation in Mn salen complexes.

Perhaps more relevant to the present discussion are the key spectroscopic differences between the two electronic configurations that exist in UV-vis-NIR, EPR and resonance Raman (rR) spectroscopies that this initial report illuminated. The UV-vis-NIR absorption spectrum of [**1**]$^+$ reveals a broad low energy band centered at 905 nm, which is similar to that for the analogous Fe(Sal) phenoxyl radical [87] (See Other Metals, Section 6). The unambiguous assignment of visible and NIR absorption transitions in the spectra of Mn(III)-phenoxyl radical [**1**]$^+$ is complicated by the presence of possibly two overlapping transitions, IVCT from L^- to $L^\bullet$ and metal-to-ligand charge transfer (MLCT) from M^{n+} to $L^{\bullet+}$. Fujii and co-workers further investigated a series of Mn(III) salen complexes in order to establish the origin of the absorption

bands in the spectra of Mn(III)-phenoxyl radical complexes [88] (Fig. 2). Evidence for a Mn(III)-phenoxyl radical electronic structure in these complexes is obvious in the ^{1}H and ^{2}H NMR spectra in which the sharp signals arising from the *tert*-butyl groups fall well outside the diamagnetic region (-3.6 and -22.0 ppm), which is indicative of a strong interaction between the *tert*-butyl groups and the paramagnetic center. In contrast, the ^{1}H NMR signals of the *tert*-butyl groups of the Mn(IV) complexes Mn(IV)(Sal)$(L)_2$ (L = CF_3CH_2O, N_3 and Cl) appear within the diamagnetic region (2.6 - 4.8 ppm), indicating only a small interaction between the Mn center and the *tert*-butyl groups [89]. Further evidence for Mn(III)-phenoxyl radical electronic structures was evident in their EPR spectra (*vide infra*).

Symmetric complexes [**4**-**6**]$^{+}$ all exhibit broad absorptions in the NIR region of their respective UV-vis-NIR spectra (7,870, 6,760, and 6,620 cm^{-1}, respectively) (Fig. 3). In order to strictly assign these as IVCT absorptions, asymmetrically substituted complexes **7** and **8** were prepared. The NIR absorption band of [**4**]$^{+}$ shifts from 7,870 cm^{-1} to 9,850 cm^{-1} upon tert-butyl substitution in complex [**7**]$^{+}$ and to 11,235 cm^{-1} upon Cl substitution in complex [**8**]$^{+}$. Fujii and co-workers propose that the band shift to higher energy is in agreement with assignment of these bands as IVCT (phenolate → phenoxyl) as the energy would increase in the order OMe < tBu < Cl, in accordance with the shifted redox potentials of the three complexes. These complexes are thus characterized as Class II mixed-valence systems on the basis of their weakly absorbing, broad IVCT bands. Complex **6** has an additional absorption band at 15,380 cm^{-1} which is unchanged upon substitution of one phenyl group with a chloride. This demonstrates that this band originates from charge transfer from the Mn(III) to the phenoxyl radical and not IVCT between phenolate and phenoxyl radical.

Final version published in: Coordination Chemistry Reviews 352, 67-82, 2017.
https://doi.org/10.1016/j.ccr.2017.08.019

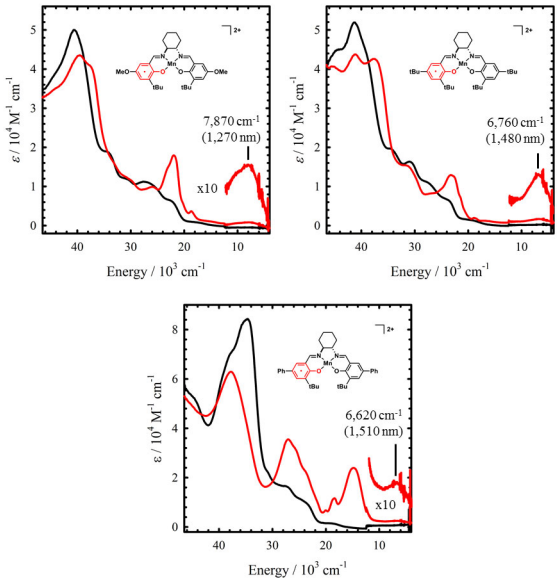

Figure 3. Absorption spectra of neutral (black lines) and one-electron-oxidized Mn complexes (red lines).

The radical localization in Mn(III) phenoxyl radical complexes with salen ligands was further investigated *via* DFT calculations [90]. The authors discuss two main factors that influence the degree of localization (or delocalization), the number of d electrons, and the energy of the metal d orbitals relative to those of the salen ligand. Oxidation to a phenoxyl radical causes the π MO (HOMO) of the phenolate to become the SOMO of the complex. Charge transfer (CT) occurs from the metal based d_π orbital into the SOMO, and increased CT (due to population of the d_π orbital) into the SOMO results in less geometric distortion between the unoxidized phenolate and phenoxyl radical which increases the delocalization of the ground-state electronic structure. This rationalization aids in comparison between Class II systems (Mn) and Class III systems (Ni). In Ni(II) d^8 complexes, the d_π orbitals are doubly occupied and thus induce more CT to the SOMO. In high-spin d^4 Mn(III) complexes, CT is also possible in the reverse direction which further increases the geometric differences between phenolate and phenoxyl radical.

Final version published in: Coordination Chemistry Reviews 352, 67-82, 2017.
https://doi.org/10.1016/j.ccr.2017.08.019

Valuable insight into the locus of oxidation in Mn salen systems can also be gained *via* EPR and rRaman spectroscopies. The EPR spectrum of [**1**]$^+$ displays two sets of signals arising from the ground and excited state Kramers doublets of an S_t = 3/2 spin system. This S_t = 3/2 spin system can be explained by considering a high-spin Mn(III) center (S_{Mn} = 4/2) interacting antiferromagnetically with a salen based ligand radical (S_{Sal} = ½), in accordance with solid-state magnetics data. The high-field signals exhibit a six-line pattern due to hyperfine interactions with the I = 5/2 ^{55}Mn nucleus (A = 82.1 and 54.8 G). The EPR spectra of symmetric and unsymmetric [**4**-**8**]$^+$ exhibit similar EPR patterns, with six-line splitting of the high-field signal due to the I = 5/2 ^{55}Mn center. The rR spectra of Mn-phenoxyl radical salen complexes can also be measured with an excitation wavelength of ~350 nm, which may correspond to the π-π* transition of the phenoxyl radical. Bands at 1,485 and 1,604 cm^{-1} in [**1**]$^+$ are assigned as ν_{7a}' and ν_{8a}' modes which consist predominantly of phenoxyl C-O and C_{ortho}-C_{meta} vibrational modes, respectively [61-63].

Recently, Clarke and Storr investigated the electronic structure and reactivity of a series of Mn(V)-salen complexes bearing terminal nitride ligands [91] (Fig. 4). Upon one-electron oxidation, complexes **9** and **10** undergo homocoupling to produce ½ equivalent of N_2 and a reduced Mn(III) product. Characterization by EPR spectroscopy reveals that the locus of oxidation in these Mn(V) complexes is not the ligand, but rather the metal, leading to reactive Mn(VI) nitride complexes which quickly undergo the observed homocoupling reaction. This reactivity has been observed in other Schiff-base containing metal complexes of Ru(VI) and Os(VI) but has not been previously observed for Mn [92-95].

Final version published in: Coordination Chemistry Reviews 352, 67-82, 2017.
https://doi.org/10.1016/j.ccr.2017.08.019

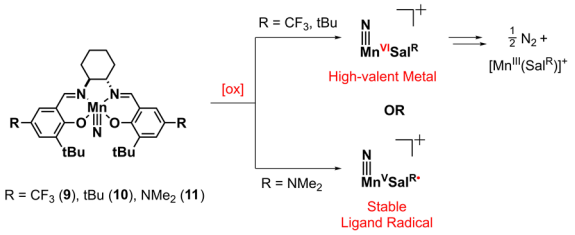

Figure 4. Mn(V) salen nitride complexes and subsequent reactivity dictated by ligand electronics upon oxidation.

Interestingly, the use of a sufficiently electron donating *para* substituent such as NMe_2 results in ligand based oxidation in **11**. The UV-Vis-NIR spectra of $[\mathbf{11}]^+$ exhibits broad, low energy absorptions centered at 6,500 (800 M^{-1} cm^{-1}) and 9,500 cm^{-1} (1,000 M^{-1} cm^{-1}) which lend to its characterization as a Class II mixed-valence complex. The room temperature EPR spectrum of $[\mathbf{11}]^+$ provides further support for a localized phenoxyl radical electronic structure as the experimental spectrum can be accurately simulated considering hyperfine interactions to only one side of the bis-phenol salen ligand. Remarkably, a shift in electronic structure also turns off the observed N-N homocoupling reactivity displayed by $[\mathbf{9}]^+$ and $[\mathbf{10}]^+$, highlighting the alternative reactivity pathways that ligand based oxidation may impose.

3. Cobalt

Much like their manganese analogues, cobalt salen complexes have widespread importance in a variety of catalytic reactions [96-102]. The most important of which are the ring opening of terminal epoxides [103-107] and the oxidation of alcohols [108-111]. In both cases, the active catalyst is a one-electron oxidized Co(II)-bis(phenolate) salen species which in principle can be described as either a Co(III)-bis(phenolate) or a Co(II)-phenoxyl radical species. Historically, the electronic structure of the active catalyst was considered to be Co(III)-bis(phenolate), however,

several elegant ^{1}H NMR and EPR investigations revealed paramagnetic behaviour in these oxidized systems [105,112-114]. Schlörer and co-workers investigated the paramagnetic behaviour of a variety of complexes of the general formula Co(Sal)X (where X = Cl, OAc, SbF_6, OTs, 3,6-difluorophenolate), reporting paramagnetic NMR spectra in non-coordinating solvents (CH_2Cl_2) and weakly coordinating solvents (THF) [113]. When the ^{1}H NMR spectra were recorded in strongly coordinating solvents like pyridine, ^{1}H NMR signals indicate a diamagnetic species. These NMR results suggest that the electronic structures of one-electron oxidized Co-salen species are strongly dependant on factors such as axial ligands, solvent and temperature. Furthermore, the magnetic susceptibility of Co(Sal)Cl (χ_i at 298 K = 0.0310 mL mol^{-1}) is in close agreement with a spin quantum number of 1, in line with an overall triplet electronic structure (*vide infra*). As a result, determining the electronic structures of one-electron oxidized Co-Sal species attracted the attention of researchers in order to improve the reactivity of active species.

Several groups have investigated the one-electron oxidation of Co(II)(Sal) complexes with a variety of experimental and theoretical techniques (Fig. 5). Thomas and co-workers studied the one-electron oxidation of compounds **12** and **13** in CH_2Cl_2 as well as in the presence of 1-methylimidazole (im) [115]. Aerobic oxidation in the presence of 1-methylimidazole results in metal-based oxidation to the octahedral Co complex **[12-(im)$_2$]$^+$** as evidenced by sharp ^{1}H NMR peaks in the diamagnetic region in $CDCl_3$. Further evidence to support metal-based oxidation exists in the solid-state structure of **[13-(im)$_2$]$^+$** in which the coordinating bonds of the salen ligand are significantly elongated (~0.05 Å) when compared to the solid-state structure of **13**. The phenolate carbon-oxygen bonds also remain unchanged when comparing between **13** and **[13-(im)$_2$]$^+$** further reflecting a metal-based oxidation process.

Final version published in: Coordination Chemistry Reviews 352, 67-82, 2017.
https://doi.org/10.1016/j.ccr.2017.08.019

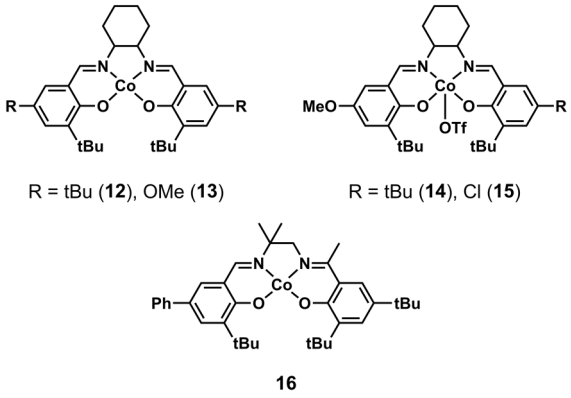

Figure 5. Co(II) salen complexes studied by various groups.

Oxidation with $AgSbF_6$ in CH_2Cl_2 results in the paramagnetic complex **[12-H_2O]**$^+$ which axially binds an adventitious water molecule during recrystallization. The Vis-NIR spectra of both **[12-H_2O]**$^+$ and **[13-H_2O]**$^+$ display NIR features (E = 9,435 cm^{-1}, ε = 5,560 M^{-1} cm^{-1}; and E = 8,200 cm^{-1}, ε = 7,370 M^{-1} cm^{-1}, respectively), which are often indicative of ligand contributions to both donor and acceptor orbitals (Fig. 6). Fujii and co-workers also reported the presence of broad NIR bands in one-electron oxidized Co(II)(Sal) complexes that are sensitive to changes in axial ligands as well as peripheral salen substituents [116]. A careful investigation of the nature of the NIR band in Co(II)(Sal) complexes by Fujii and co-workers revealed significant ligand-to-metal charge transfer character on the basis of an observed red-shift when more electron donating substituents were placed in the *para* position of the salen ligand (**14** & **15**). TD-DFT calculations on a related monomeric Co(II)(Sal) complex (**16**) by Storr and co-workers agreed with this assignment, in which the low-energy transition was predominantly ligand-to-metal charge transfer [117]. Synthesis of asymmetric Co(II)(Sal) derivatives by Fujii and co-workers revealed a small but consistent temperature dependence of the NIR feature. They postulate that ligand-to-ligand charge transfer of the [Co(II)(Sal•)]$^+$ electronic structure overlaps with the ligand-to-metal charge transfer of the Co(III)(Sal) electronic structure. Further evidence of both

electronic structures contributing to the overall electronic structure can be found in magnetic and DFT studies (*vide infra*).

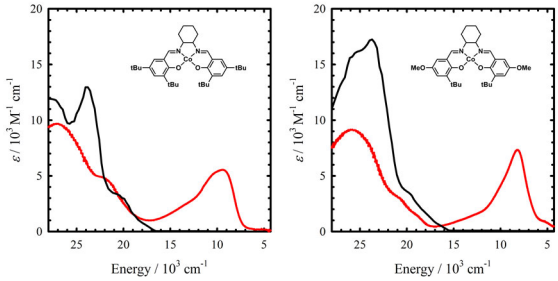

Figure 6. Absorption spectra of **12-13** (black lines) and [**12-H$_2$O**]$^+$ and [**13-H$_2$O**]$^+$ (red lines).

Solid-state magnetism data reported by Storr and co-workers and Fujii and co-workers on related oxidized monomeric Co(II)(Sal) complexes is consistent with the contribution of two electronic structures [116,117]. The reported magnetic data is consistent with both a Co(II)(Sal•+) as well as a high-spin Co(III)(Sal) electronic structure. Interestingly, the solid-state magnetic data suggests weak antiferromagnetic coupling between the Co(II) ion and the ligand-based radical (J = -5 cm^{-1}) in this electronic structure. In contrast to these results, solid-state magnetic data reported by Thomas and co-workers suggests a high-spin Co(II) center strongly antiferromagnetically coupled to a phenoxyl radical [115]. This discrepancy highlights the sensitivity of these one-electron oxidized systems to packing in the solid-state and/or differences in donating ability of the salen and axial ligands employed.

DFT calculations on these systems also provided further insight into the overall electronic structures. Both Storr and co-workers as well as Thomas and co-workers investigated the electronic structures by theoretical methods and reported a triplet electronic structure as lowest in energy [115,117]. This triplet electronic structure can originate from either a high-spin Co(III)(Sal) system or a low-spin Co(II)(Sal•+) in which the ligand-based radical is coupled

ferromagnetically to the Co(II) center. The unpaired spin density reported by both groups resides predominantly on the Co metal center (~70%) with the remaining spin delocalized across the ligand framework. The TD-DFT results obtained by Storr and co-workers reproduce the experimentally observed NIR band at 8,500 cm^{-1} and the predicted transition is largely ligand-to-metal charge transfer in character, in good agreement with the assignment made by Fujii and co-workers. However, it should be noted that the calculated electronic structures are nearly isoenergetic, which lends support to the postulation by Fujii and co-workers that the NIR features in these complexes are a combination of metal-to-ligand charge transfer (from Co(III)(Sal)) as well as ligand-to-ligand charge transfer (from $Co(II)(Sal\bullet)^{+}$).

Double oxidation of monomeric Co(II)(Sal) complexes by Thomas and co-workers (electrochemical oxidation) and Storr and co-workers (chemical oxidation) leads to genuine Co(III)(phenoxyl radical) electronic structures [115,117]. The EPR spectra for these doubly oxidized species is consistent with an $S = ½$ spin system with signals centered at $g = 2.00$. DFT calculations on the doubly oxidized species also reflect the electronic structure as a localized Co(III)-phenoxyl radical with the spin density residing predominantly on one side of the salen ring. Earlier studies by Van Doorslaer and co-workers on double oxidation of Co(II)(Sal) complexes in the presence of acetic acid and air also showed evidence for genuine Co(III)(phenoxyl radical) electronic structures *via* both EPR and computational methods [112].

Finally, while oxidation of metal salen complexes has been extensively investigated, a recent report highlighted the reduction of Co(II) salen complexes using various alkali metals, as well as their reactivities with CO_2 [118]. The use of Li and Na as strong reductants resulted in ligand based reduction and dimerization through the salen imine functionalities, while employing K as

the reductant resulted in metal-based reduction to Co(I). Multiple CO_2 reduction products were detected, including CO_3^{2-} in 53% yield.

4. Nickel

The most extensively studied of the one-electron oxidized metal salen complexes are those of nickel. The square planar coordination environment imposed by the salen ligand results in diamagnetic Ni(II) ground state which upon one-electron oxidation forms a doublet (S = ½) spin state. EPR spectroscopy is routinely employed to determine the locus of oxidation in these systems (either metal or ligand); while NIR spectroscopy is an invaluable tool for determining the overall localization/delocalization of the electron hole. Secondary techniques such as rR, cyclic voltammetry (CV) and theoretical calculations are also key to elucidating the electronic structure of these systems. Oxidized Ni salen complexes have recently been elegantly reviewed by Thomas [119], and as such our discussion will be largely focused on structural features that influence the degree of delocalization/localization of the unpaired electron.

Early electrochemical oxidation of Ni salen complexes were performed in coordinating solvents such as DMF/DMSO and in all cases Ni(III) EPR signals were observed [39,120,121]. Isolation of a Ni(II) salen radical was first achieved in 1996 by Peng and co-workers [122], who postulated that initial formation of a Ni(III) species followed by internal electron transfer resulted in the observed stable Ni(II) salen radical. After this initial isolation, a few reports focusing on an apparent temperature dependent valence tautomerism between Ni(II) salen radical and Ni(III) phenolate electronic structures emerged [61,123,124]. However, in 2007, two reports described the temperature independence of the Ni(II) salen radical electronic structure [64,125], and attributed the previously observed temperature dependent valence tautomerism to different oxidation protocols (the use of ligating vs. non-ligating counterions) as well as the axial binding

Final version published in: Coordination Chemistry Reviews 352, 67-82, 2017.
https://doi.org/10.1016/j.ccr.2017.08.019

of water (or other impurities) at the solvent freezing point. It was thus concluded that in the absence of axial donors, oxidation of Ni(II) salen complexes results in a phenoxyl radical electronic structure. The Ni salen complexes discussed herein will fall broadly into one of two categories, those with aliphatic diamine bridges or those with aromatic diamine bridges; we will also discuss symmetric ($R_1 = R_2$) and asymmetric ($R_1 \neq R_2$) ligand systems separately (Figs. 7 and 10).

4.1 Aliphatic Diamine Bridges

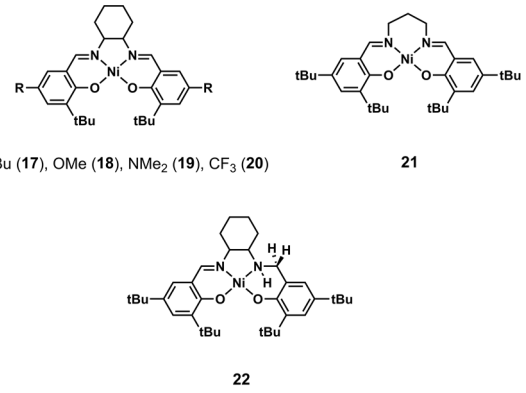

Figure 7. Symmetric and asymmetric Ni salen complexes with aliphatic diamine bridges.

The first structurally characterized Ni salen-phenoxyl radical complex, $[\mathbf{17}]^+$, was reported in 2007 [64]. Relative to its neutral analogue, $[\mathbf{17}]^+$ possesses a contracted coordination sphere by ~0.02 Å which is attributed to removal of an electron from a largely ligand-based π^* orbital. More interestingly, the contraction is symmetric suggesting a delocalized electronic structure. In contrast, the X-ray structure of $[\mathbf{18}]^+$ exhibits an asymmetric coordination sphere, with a quinoid distribution of bond lengths on one side of the ligand, which suggests radical localization in this derivative (*vide infra*) [126].

Final version published in: Coordination Chemistry Reviews 352, 67-82, 2017.
https://doi.org/10.1016/j.ccr.2017.08.019

Complexes **19** and **20** were also prepared, in order to investigate the influence of the phenolate *para* substituent on the overall electronic structure upon oxidation [58,127]. [**17**-**20**]$^{+}$ all exhibit low energy features in the NIR region of their respective UV-Vis-NIR spectra (Fig. 8). [**17**]$^{+}$ and [**20**]$^{+}$ are characterized as fully delocalized Class III systems on the basis of their intense NIR bands at 4700 cm^{-1} (ε = 21,500 M^{-1} cm^{-1}, $\Delta\nu_{1/2}$ = 660 cm^{-1}) and 4,900 cm^{-1} (ε = 16,200 M^{-1} cm^{-1}, $\Delta\nu_{1/2}$ = 660 cm^{-1}) for [**17**]$^{+}$ and [**20**]$^{+}$, respectively.

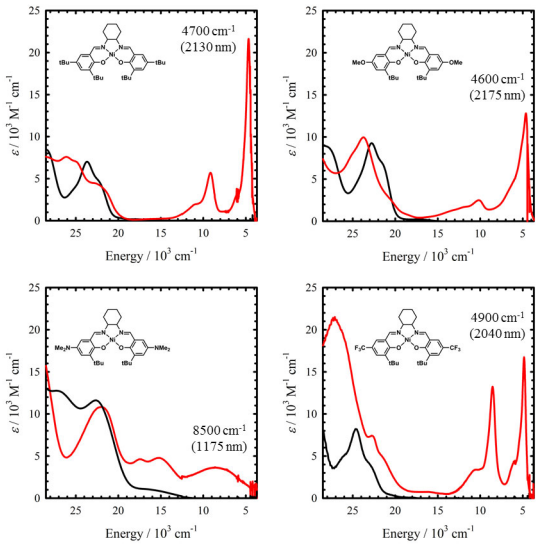

Figure 8. Absorption spectra of **17**-**20** (black lines) and [**17**-**20**]$^{+}$ (red lines).

This is further complimented by DFT calculations, in which the orbitals involved in the low-energy transitions are predicted to be predominantly ligand-based, and delocalized across the entire ligand framework [127,128]. The NIR band of [**18**]$^{+}$ appears at 4600 cm^{-1} (ε = 12,700 M^{-1} cm^{-1}, $\Delta\nu_{1/2}$ = 1,250 cm^{-1}) and is broader in comparison to the more electron deficient [**17**]$^{+}$ and [**20**]$^{+}$. This data, combined with DFT calculations, rR spectroscopy, and the asymmetric coordination sphere observed in the solid state, leads to the characterization of [**18**]$^{+}$ as a borderline Class III/II system. In a separate paper [88], Kurahashi and Fujii report the UV-Vis-

NIR spectra of [**18**]$^+$ as having a much broader NIR band than that reported by Storr and co-workers ($\Delta\nu_{1/2}$ = 2,900 cm^{-1}) which is likely attributed to the presence of excess supporting-electrolyte due to electrochemical oxidation. This difference highlights the sensitivity of the resultant oxidized salen electronic structures to factors such as solvent, and identity and concentration of the counterion. Lastly, the NIR band of [**19**]$^+$ appears at higher energy relative to the other three complexes (8,500 cm^{-1}) and is significantly broader (ε = 3,600 M^{-1} cm^{-1}, $\Delta\nu_{1/2}$ = 6,650 cm^{-1}), and solvent dependent, highlighting the assignment of [**19**]$^+$ as a localized Class II mixed-valence species. This derivative is predicted to have the most localized SOMO of the series by DFT, with the MOs involved in the observed IVCT band reflecting a charge transfer from a phenolate to phenoxyl sides of the salen ligand.

Furthermore, the EPR spectra of complexes [**17**-**20**]$^+$ reflect a decreased spin density on the Ni(II) center as the electron donating ability of the *para* substituent increases. The g_{av} values for complexes in which the SOMO has a non-negligible contribution from the central Ni ion are greater than that for the free electron, and move closer to the free electron value as the metal character of the SOMO decreases (g_{av} = 2.067 [**20**]$^+$ > 2.045 [**17**]$^+$ > 2.023 [**18**]$^+$ > 2.004 [**19**]$^+$) [58,64,127]. Theoretical calculations reproduce this experimental result, with decreased metal contribution to the SOMO of the Ni complexes (Fig. 9) as the electron donating ability of the substituent increases (SD_{Ni} = 34% [**20**]$^+$ > 16% [**17**]$^+$ > 4% [**18**]$^+$ > 2% [**19**]$^+$). Due to the tendency of DFT to favor symmetrically delocalized structures [58,66], the Coulomb-attenuated method (CAM-B3LYP) was used in place of B3LYP. Using the CAM-B3LYP functional, short and long range interactions are modelled with differing combinations of Hartree-Fock (HF) and Becke1988 [66,129,130], and this functional correctly predicts the electronic structure in [**17**-**20**]$^+$ Taken together with the EPR and UV-Vis-NIR data, it is postulated that participation of the

NMe_2 and OMe groups in the localization of the electron hole provides a stabilization pathway other than delocalization through the central Ni ion. This stabilization mechanism was further investigated with a tris(methoxy) substituted Ni salen complex in which the resultant electronic structure is also localized to one side of the salen ligand, with experimental studies and theoretical calculations suggesting an overall Class II mixed valence species [131]. In all cases, addition of pyridine results in complete loss of the NIR features and a shift in the g_{ave} values to $g_{av} > 2.15$, reflecting an intramolecular electron transfer from Ni(II) to phenoxyl radical, resulting in an octahedral Ni(III) species. Well resolved 5 line patterns in the high field portion of the EPR spectrum is diagnostic of 2 molecules of pyridine binding in the axial positions of the Ni(III) ion ($S_N = 1$) in these derivatives.

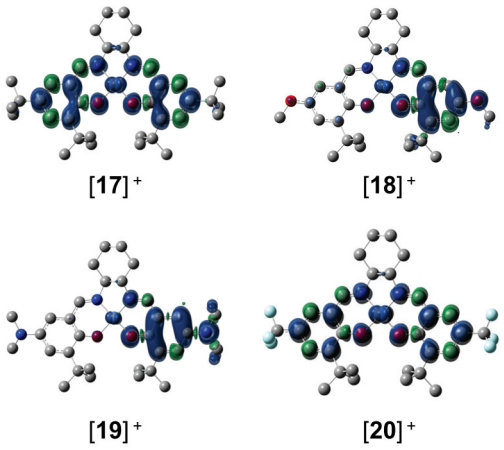

Figure 9. DFT spin density (SD) plots for [**17**-**20**]$^+$ calculated using the CAM-B3LYP functional. See the text for spin density distributions.

Finally, double oxidation of **17** to [**17**]$^{2+}$ results in a bis-ligand radical species in which the delocalized spin in [**17**]$^+$ becomes localized upon further oxidation [132]. Double oxidation in the presence of pyridine results in a Ni(III)-phenoxyl radical species [133].

The effect of the chelate bridge on the electronic structure of oxidized Ni salen complexes has also been investigated [134]. Ni salen with a 6-membered chelate bridge (**21**) exhibits greater flexibility in comparison to its 5-membered analogues (ethylenediamine / cyclohexanediamine) which results in subtle differences in electronic structure of the oxidized forms. Like [**17**]$^+$, [**21**]$^+$ exhibits a symmetrically contracted coordination sphere in the solid state, suggesting a delocalized electronic structure. The NIR band for one-electron oxidized [**21**]$^+$ is shifted to lower energy in comparison to that of [**17**]$^+$ (4300 cm^{-1} vs 4500 cm^{-1}) and is of lower intensity (17,500 M^{-1} cm^{-1} vs 21,500 M^{-1} cm^{-1}). While still a Class III mixed valence complex ($\Delta\nu_{1/2}$ < 1,000 cm^{-1}), the lower energy and intensity of the NIR band for [**21**]$^+$ in comparison to [**17**]$^+$, likely reflects an increased distortion from a square planar geometry and less effective overlap between the Ni d_{xz} orbital and the appropriate ligand MO in [**21**]$^+$. Unlike the 5-membered chelate bridges studied previously, which form Ni(III)-phenoxyl radical species upon double oxidation, [**21**]$^{2+}$ in the presence of pyridine results in a high-spin Ni(II)-bis(phenoxyl radical) species [133]. This is likely due to the increased flexibility (and longer coordination bond lengths) of the 6-membered chelate being able to stabilize the bis-phenoxyl electronic structure.

Reduction of one of the imine functionalities of **17** to an amine results in the asymmetric complex **22** [60]. Preferential oxidation of the more electron-rich aminophenolate moiety results in the localized phenoxyl radical [**22**]$^+$. Unlike the symmetric coordination sphere contraction observed for [**17**]$^+$, the crystal structure of [**22**]$^+$ is asymmetric, with the aminophenolate Ni-O bond lengthening by 0.04 Å – attributable to the decrease in electron-donating ability of a phenoxyl ligand vs. a phenolate. rR further highlights the localization of the ligand-based radical as both phenoxyl and phenolate vibrational modes are present in the spectrum. The NIR features

Final version published in: Coordination Chemistry Reviews 352, 67-82, 2017.
https://doi.org/10.1016/j.ccr.2017.08.019

are consistent with a Class II mixed valence species (E = 6,500 cm^{-1}, ε = 2,000 M^{-1} cm^{-1}) due to limited coupling between the redox-active phenolate moieties in [**22**]$^+$.

4.2 Aromatic Diamine Bridges

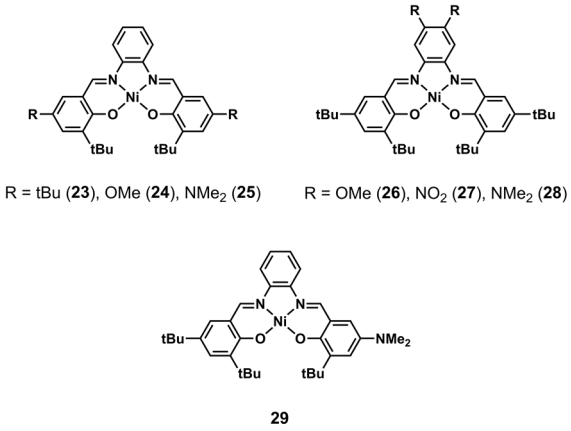

Figure 10. Symmetrical and asymmetrical Ni salophen complexes.

The UV-Vis-NIR spectrum for the one-electron oxidized Ni salophen complex [**23**]$^+$ exhibits a NIR band at 3,600 cm^{-1} (ε = 3,700 M^{-1} cm^{-1}, $\Delta\nu_{1/2}$ = 2,400 cm^{-1}) which is of lower energy and significantly lower intensity in comparison to the analogous cyclohexanediamine complex [**17**]$^+$ (E = 4,500 cm^{-1}, ε = 21,500 M^{-1} cm^{-1}) [135]. The NIR band shift to lower energy is a result of less metal character (DFT calculated 14.5% vs. 16.4%) which leads to less metal-ligand antibonding in the β-LUMO, resulting in a decrease in the β-HOMO → β-LUMO energy gap. This is further reflected in the decreased g_{av} value of 2.027 for [**23**]$^+$ vs. 2.045 for [**17**]$^+$ in the respective EPR spectra. Interestingly, simply switching from a cyclohexanediamine backbone to a conjugated *o*-phenylenediamine backbone results in a near 6-fold decrease in the intensity of the experimentally observed NIR band. Inspection of the predicted donor and acceptor orbitals for the low-energy transition of [**23**]$^+$ reveals participation of the *o*-phenylenediamine backbone which adds increased intraligand CT character. NIR band analysis leads to the assignment of

[**23**]$^{+}$ as a borderline Class II/III mixed valence species. Replacement of the *para* tBu substituent with the more electron donating substituents OMe and NMe_2 results in electronic structure changes as detailed previously for the cyclohexanediamine backbone complexes [136]. While the NIR spectra were not recorded beyond 1100 nm, a sequential decrease in the g_{av} values (2.034 [**23**]$^{+}$ > 2.017 [**24**]$^{+}$ > 2.006, [**25**]$^{+}$) reflects a similar decrease in Ni contribution to the SOMO as observed for the aliphatic analogues.

Decoration of the *o*-phenylenediamine backbone with OMe (**26**), NO_2 (**27**) or NMe_2 (**28**) groups at the two positions *para* to the amine functionalities also has implications on the observed electronic structures [137,138]. The mildly electron-donating OMe group results in oxidation at the bis-phenolate portion of the ligand, similarly to [**23**]$^{+}$ [137]. The more strongly electron-donating NMe_2 group in **28** however, results in the first and second oxidation events taking place on the neutral *o*-phenylenediamine bridge [138]. In the case of **27**, with two electron withdrawing NO_2 groups, a singly oxidized product could not be isolated due to disproportionation into the neutral and dicationic forms. Oxidation in the presence of pyridine stabilized the disproportionation, but resulted in an oxidation locus at the metal center to form Ni(III) [137]. These results highlight that the electronic structures of Ni salen systems are not only sensitive to substitution around the phenolate moieties, but also on the bridging group.

Replacement of one of the *para* tBu groups in **23** with an NMe_2 group results in an asymmetric complex **29** which is preferentially oxidized on the more electron rich NMe_2 side of the bis-phenol ligand [139]. Protonation of the NMe_2 group however, shifts the locus of oxidation from the NMe_2 side of the ligand, over to the tBu substituted side. The EPR spectrum for the NMe_2 complex displays a g_{av} value of 2.01 with significant hyperfine splitting attributable to the 6 protons and 1 nitrogen of the NMe_2 group. The EPR spectrum for [**29-H**]$^{2+}$ however has

Final version published in: Coordination Chemistry Reviews 352, 67-82, 2017.
https://doi.org/10.1016/j.ccr.2017.08.019

no observable hyperfine splitting and a slightly higher g_{ave} value of 2.02 – which may reflect an increased contribution of the Ni ion to the SOMO.

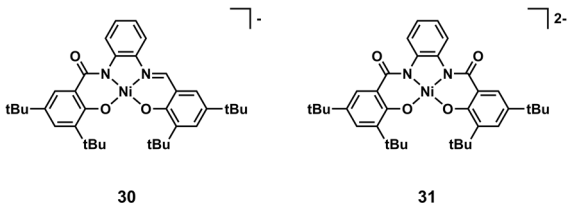

30 31

Figure 11. Replacement of the imino functionalities of **23** with one (**30**) and two (**31**) amido donors.

Sequential replacement of the imino nitrogen donors with anionic amido nitrogen donors has a significant effect on the overall electronic structure of the one-electron oxidized species (Fig. 11). Replacement of one imino functionality in **30** results in oxidation on the more electron rich amido side of the bis-phenol ligand and the NIR features appear at higher energy (4,400 cm^{-1}) and are broader (ε = 2,260 M^{-1} cm^{-1}) in comparison to [**23**]$^+$. The NIR data, and TD-DFT predicted donor and acceptor orbitals reflecting phenolate to phenoxyl charge transfer suggests [**30**]$^+$ is best described as a Class II species. Replacement of both imino functionalities with amido groups in **31** results in an electronic structure with metal contribution that is the highest in the series. The NIR band shifts to even higher energy (5,900 cm^{-1}) and is considerably broader than the other two complexes in the series (ε = 940 M^{-1} cm^{-1}). Interestingly, TD-DFT calculations predict the orbitals involved in the transition to have significant ligand-to-metal charge transfer character. Along with the redox-active phenolate moieties, the dianionic bridge is also redox-active in **31** and can contribute to the overall electronic structure of the one-electron oxidized form. This is reflected in the DFT generated SOMO in which significant spin density

can be found on the deprotonated aromatic bridge resulting in the electronic structure of this complex being best described as a hybrid phenoxyl / aminyl complex.

Overall, Ni salen systems are good model complexes for testing the Robin-Day classification system for delocalization. UV-Vis-NIR spectroscopy is an invaluable technique as the observed NIR bands are an excellent spectroscopic marker to the degree of delocalization of the resultant electron hole after one-electron oxidation.

5. Copper

The significant interest in oxidized Cu salen complexes arises from their use as both structural, and in some cases, functional, models of the enzyme galactose oxidase (GO_{ase}) (see Introduction). The relatively stable yet reactive Cu-phenoxyl form of oxidized Cu salen complexes has allowed for an increased understanding of both the reactivity, and spectroscopic signatures of the oxidized form of GO_{ase} (GO_{ox}, see Scheme 1).

Stack [19,27], Wieghardt [140,141], and Thomas [142] have provided critical insights into the electronic structure and reactivity of phenoxyl radical-coordinated Cu complexes, and relationship to the GO_{ase} enzyme. A recent review in this journal by Lyons and Stack details the use of salen-type complexes as mixed-valent GO_{ase} models [27], and thus we will focus the discussion here on selected compounds and electronic structures in this review.

In 1996, Stack and co-workers elucidated the structural features necessary for GO_{ase} reactivity through functional group variation of a series of complexes (**32**-**34**) (Fig. 12) [19,143]. These compounds were effective for the catalytic transformation of benzyl alcohol to benzaldehyde with > 1,000 turnovers under mild conditions. Further analysis of the neutral and oxidized forms

Final version published in: Coordination Chemistry Reviews 352, 67-82, 2017.
https://doi.org/10.1016/j.ccr.2017.08.019

by Cu K-edge and X-ray absorption spectroscopy (XAS), showed that the Cu(II) center remains unchanged upon oxidation, confirming phenoxyl radical formation.

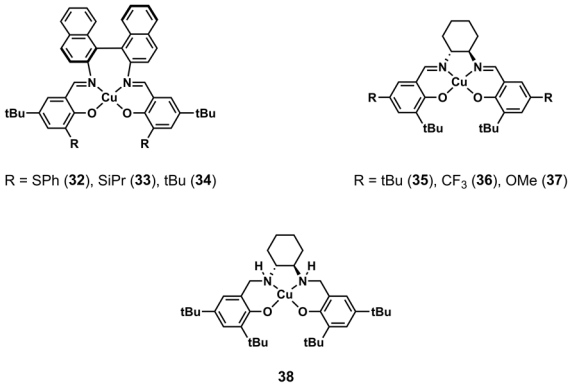

Figure 12. Initial Cu salen complexes studied as functional mimics for GO_{ase}.

The oxidation and comparative reactivity of **35** and **38** (containing a reduced salen ligand) have been extensively investigated [30,65,144,145] (Fig. 12). Initial studies showed that both oxidized complexes react with the model substrate benzyl alcohol to form benzaldehyde, however compound [**38**]$^+$ reacts more quickly despite being a weaker oxidant ($E_{1/2}$ is 80 mV for **38** and 450 mV for **35**, vs. Fc^+ / Fc). A mechanistic difference was uncovered in which initial substrate binding to [**38**]$^+$ likely results in more rapid reactivity. Subsequent in-depth characterization of the electronic structure of [**35**]$^+$ demonstrated that the complex exists as two essentially isoenergetic valence tautomers at 298 K, a triplet Cu(II)-phenoxyl radical species, and a diamagnetic Cu(III) species. In the solid state, and at low temperatures, the Cu(III) electronic structure is stabilized as deduced by XAS, X-ray photoelectron spectroscopy (XPS), X-Ray crystallography, rR and magnetic measurements. Variable temperature UV-vis-NIR, and solution susceptibility measurements confirmed the presence of both valence tautomers in a *ca.* 1:1 ratio at 298 K. The shift to the high-valent Cu(III) species at low temperature is similar to the temperature-dependent valence tautomerism observed in a number of metal-dioxolene

complexes [146-150]. Thus, the slower reactivity for [**35**]$^+$, in comparison to [**38**]$^+$ is likely due to the presence of the Cu(III) tautomer, which disfavours axial substrate binding in comparison to the Cu(II) d^9 species [144]. Substrate preorganization *via* substrate binding allows enzymes such as GO_{ase} to perform highly selective transformations under mild conditions. In the case of the analogous Ni(II) ligand radical species, axial binding results in a shift in the locus of oxidation from ligand to metal, forming an octahedral d^7 Ni(III) complex (see Section 4) [61,64,127].

Further investigation of the *para*-CF_3 (**36**) [127] and *para*-OMe (**37**) [126] substituted analogues shows the effect of peripheral ligand electronics on the electronic structure of the oxidized forms. For [**36**]$^+$, oxidation affords a temperature-invariant Cu(III) species under the conditions studied due to the electron-poor salen ligand. Employing the more electron-rich *para*-OMe substituents in [**37**]$^+$ results in a triplet Cu(II)-phenoxyl radical species in solution and in the solid state [31]. Further evaluation of the bond lengths in the solid-state structure of [**37**]$^+$ shows that the radical is localized, similarly to the Ni derivative (*vide supra*). Comparative DFT spin density plots (Fig. 13) for [**35**]$^+$ and [**37**]$^+$ show localization on one of the phenolates for [**37**]$^+$, in accord with the experimental data.

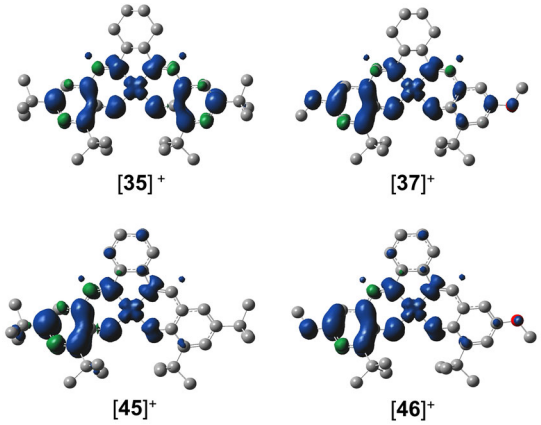

Final version published in: Coordination Chemistry Reviews 352, 67-82, 2017.
https://doi.org/10.1016/j.ccr.2017.08.019

Figure 13. DFT Spin Density (SD) plots for [**35**]$^+$, [**37**]$^+$, [**45**]$^+$, and [**46**]$^+$ using the B3LYP functional. Note for [**35**]$^+$ this is the SD for the triplet valence tautomer.

UV-vis-NIR spectroscopy has been an extremely useful technique for detecting the presence of low energy IVCT bands in GO_{ase} model complexes. For example, GO_{ox} displays an envelope of low energy transitions at *ca*. 12,500 cm^{-1} [151]. NIR absorptions for [**35**]$^+$ and [**37**-**38**]$^+$ (shown in Fig. 14) are assigned to phenolate-phenoxyl IVCT bands on the basis of both experimental and theoretical analysis [30,31,127]. Interestingly, band shape analysis of the NIR absorptions for [**35**]$^+$ and [**37**-**38**]$^+$ (Fig. 14) shows Class II behavior, despite the structural differences. The LMCT band for [**35**]$^+$ at 18,000 cm^{-1} doubles in intensity with decreasing temperature, due to temperature-dependent equilibrium between Cu(II) and Cu(III) species in solution [65]. An expanded study by Stack and co-workers [31,145], including both symmetric and asymmetric substituted analogues (**39**-**44**, Fig. 15), shows similar Class II character. However, use of a thioether ring substituent has provided insight into the stabilizing role of this substituent, including radical delocalization onto sulfur [31,145]. Overall, comparing the Ni(II) and Cu(II) data shows key differences in experimentally observed NIR transitions, and degree of radical delocalization based on the central metal ion.

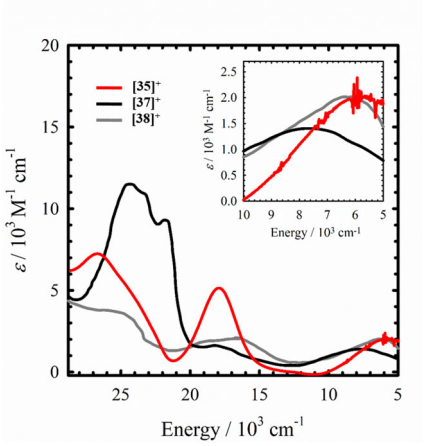

Final version published in: Coordination Chemistry Reviews 352, 67-82, 2017.
https://doi.org/10.1016/j.ccr.2017.08.019

Figure 14. Absorption spectra of [**35**]$^+$ (grey line), [**37**]$^+$ (black line), and [**38**]$^+$ (red line)

Thomas and co-workers initially examined the potential participation of a bridging phenylenediamine moiety in the electronic structure of [**45**]$^+$, due to the planarity and conjugation of the backbone [33]. The electronic structure investigations were then continued by Shimazaki, Ottenwaelder and Thomas [152,153] by varying the electron-donating character of both phenolates (**45** and **46**) and phenylenediamine backbone (**47** and **48**). The oxidized forms were characterized by both experimental and theoretical methods to be a Cu(II)-phenoxyl radical ([**45**]$^+$ and [**46**]$^+$) or a Cu(II)-*o*-diiminobenzene radical ([**47**]$^+$ and [**48**]$^+$) [152-154].

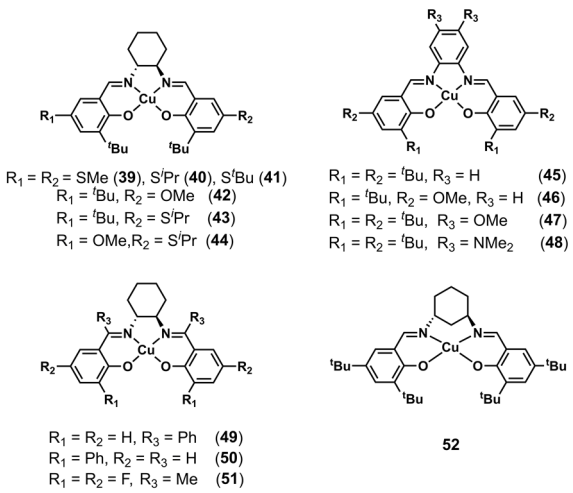

Figure 15. Symmetric and asymmetric Cu salen complexes with aliphatic and aromatic diamine bridges.

Characterization of [**45**]$^+$ supports a phenoxyl radical species in the solid-state, whereas in solution, the experimental data suggests slight changes in electronic structure dependent on the phase [152]. In addition, DFT calculations support changes to the degree of delocalization based on the amount of interaction between [**45**]$^+$ and the counterion. A comparison of the predicted spin density for [**35**]$^+$ and [**45**]$^+$ (Fig. 13) at the same level of theory supports localization of the

ligand radical on one side of the molecule for [**45**]$^+$ with significant participation of the phenylenediamine unit in comparison to 1,2-cyclohexanediamine. A similar electronic structure is predicted for [**46**]$^+$ with significant participation of the phenylenediamine backbone in comparison to [**37**]$^+$ (Fig. 13). Participation of the phenylenediamine in the SOMO is expected based on the planar π system, and the differences in electronic structure compared to the aliphatic backbone analogues could be related to non-planar deformations also observed in porphyrin π cation radicals [155].

The functionalization of the phenylenediamine moiety with electron donating OMe (**47**) and NMe_2 (**48**) groups results in delocalization of the ligand radical across three aromatic rings for [**47**]$^+$, and localization of the ligand radical on the aromatic bridge for[**48**]$^+$ [153,154]. TD-DFT calculations predict low-energy intraligand charge transfer (ILCT), as opposed to IVCT, for [**48**]$^+$.

The reactivity profile for the oxidation of benzyl alcohol using [**45**-**47**]$^+$ varies across the series, even though similar yields (*ca.* 50%) were achieved. Complex [**45**]$^+$ followed a bimolecular reaction process with similar reactivity to [**35**]$^+$, even through the electronic structure differs. Both [**46**]$^+$ and [**47**]$^+$ exhibit slower reactivity in comparison to [**45**]$^+$, with only electron transfer and no hydrogen atom abstraction as part of the mechanistic process [154]. Even though the oxidation potential of **48** compared to **45** is significantly lower (by *ca*. 0.5 V), [**48**]$^+$ is competent in benzyl alcohol oxidation [153].

The redox chemistry of copper salen-type complexes (**49**-**51**) with functional group substitution on both the phenolate and imine moieties was recently investigated by Klein and co-workers [156]. Complexes **49** and **51** showed reversible one-electron oxidation processes, with [**49**]$^+$ displaying UV-vis bands consistent with phenoxyl radical formation. The oxidized forms

were found to be unstable likely due to the lack of *ortho* and/or *para* protecting groups. The authors did not characterize the oxidized forms; however preliminary catalytic benzyl alcohol oxidation trials afforded limited reactivity in comparison to established Cu catalysts.

The 5-membered chelate backbone in the majority of salen-type ligands governs the metal coordination sphere geometry and hence the ability to sustain various oxidation states. Extending the chelate backbone introduces increased flexibility to these ligands allowing for distortion away from a planar ligand framework, thus supporting alternate metal coordination sphere geometries such as tetrahedral for Cu(I). As an example, Shimazaki and co-workers investigated the electronic structure of [**52**]$^+$ (a 6-membered backbone chelate), and related their findings to previously well-characterized [**35**]$^+$ [157]. Solid-state characterization together with XPS, magnetic susceptibility, EPR, and rR measurements were consistent with a localized phenoxyl radical complex and a triplet groundstate [157]. The presence of a weak and broad NIR band for [**52**]$^+$ (6,600 cm^{-1}, ε_{max} = 920 M^{-1} cm^{-1}, $\Delta\nu_{1/2}$ = 1,430 cm^{-1}) confirms the formation of localized phenoxyl radical species and hence can be best described as a Class II mixed-valence complex. Reactivity studies with benzyl alcohol indicated that [**52**]$^+$ likely undergoes similar mechanistic steps as [**35**]$^+$, but at a faster rate. The increased flexibility of the 6-membered ring in [**52**]$^+$ may allow for enhanced interaction with the substrate, as well as access to the Cu(I) oxidation state, compared to [**35**]$^+$ [157].

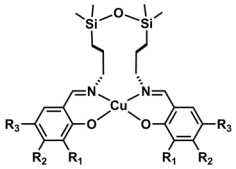

$R_1 = R_2 = R_3 = H$ (**53**)
$R_1 = R_3 = Br$, $R_2 = H$ (**54**)
$R_1 = R_3 = H$, $R_2 = OH$ (**55**)
$R_1 = R_2 = H$, $R_3 = NO_2$ (**56**)
$R_1 = R_2 = H$, $R_3 = Cl$ (**57**)

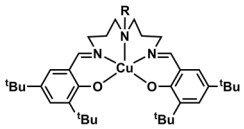

R = CH_3 (**58**)
R = H (**59**)

Final version published in: Coordination Chemistry Reviews 352, 67-82, 2017.
https://doi.org/10.1016/j.ccr.2017.08.019

Figure 16. Cu salen complexes with extended siloxane backbones (left) and pentadentate Cu salen complexes (right).

The synthesis of a series of Cu(II) Schiff-base complexes (**53-57**) with an extended twelve-membered siloxane backbone were reported by Arion and co-workers [158] (Fig. 16). Even though the electronic structure of the oxidized forms of **53-57** were not investigated, these complexes were tested as benzyl alcohol oxidation catalysts in the presence of the TEMPO radical (2,2,6,6-tetramethylpiperdine-1-oxyl), affording high catalytic activity and selectivity. The authors proposed that a Cu(I) species is generated upon reduction with radical substrate, which is in line with the reduced form of GO_{ase}.

Finally, McMaster and Schröder reported the synthesis and characterization of **58** and **59** with Schiff-base ligands containing a modified backbone, affording a pentadentate N_3O_2 coordination sphere [159] (Fig. 16). Spectroelectrochemical oxidation of **58** and **59** resulted in the generation of a broad absorption band at 720 nm for both complexes, which was assigned to a phenoxyl radical [160]. Owing to the coupling of the copper unpaired electron ($S = ½$) and the phenoxyl ligand radical ($S = ½$), samples of $[\mathbf{58}]^+$ and $[\mathbf{59}]^+$ were EPR silent at 273 and 77 K. However, doubly oxidized samples ($[\mathbf{58}]^{2+}$ and $[\mathbf{59}]^{2+}$) at 77 K gave rise to isotropic signals ($g = 2.008$ and 2.009, respectively) further confirming ligand-based oxidation for these complexes [159].

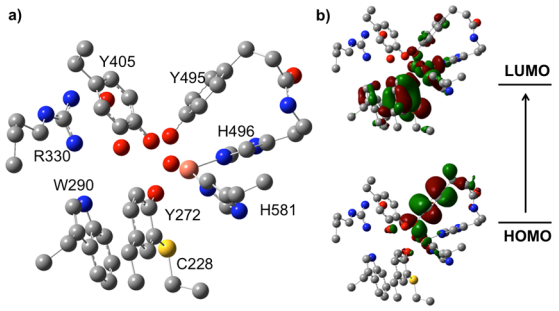

Final version published in: Coordination Chemistry Reviews 352, 67-82, 2017.
https://doi.org/10.1016/j.ccr.2017.08.019

Figure 17. a) GO_{ase} model investigated; b) TD-DFT predicted low energy IVCT at *ca*. 6,000 cm^{-1} (HOMO → LUMO) for oxidized GO_{ase}.

The search for functional Cu complexes that mimic aerobic oxidation of alcohols by GO_{ase} continues. An elegant computational study on GO_{ox} has improved our understanding of the electronic structure and reactivity of this enzyme [151]. Further calculations using this GO_{ase} model (Fig. 17a) predict a low energy IVCT band (5,977 cm^{1}) that has yet to be investigated experimentally. Intriguingly, the predicted band is an excellent match with the NIR bands experimentally observed for oxidized Cu salen systems (Fig. 17b), highlighting the utility of the salen framework as a model system for GO_{ase}.

6. Other Metals

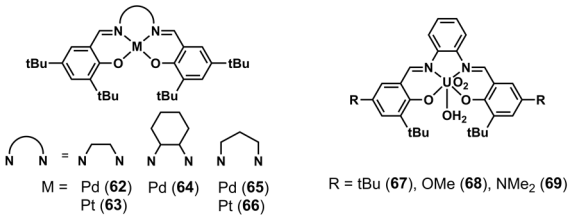

Figure 18. Salen ligands coordinated to metals other than those previously described.

The synthesis and electronic structure determination of oxidized salen-type ligands with metal ions other than those detailed in previous sections are briefly described here (Fig. 18). As a model for iron-containing enzymes, the electronic structure and reactivity of sterically hindered Fe(III) salen complexes (**60** (X = Cl) and **61** (X = H_2O)) analogous to **1** (Fig. 2) have been examined by Fujii and co-workers [87]. Singly oxidized forms of **60** and **61** afford Fe(III)-phenoxyl radical species, based on UV-Vis, EPR and rR measurements. [**60**]$^+$ and [**61**]$^+$ displayed only minimal reactivity towards benzyl alcohol oxidation.

Pd(II) and Pt(II) salen complexes, **62-66** (analogues to Ni complexes **17** and **21**) have also been described [64,128,134,161]. A localized Pd(II)-phenoxyl/phenolate electronic structure was determined for [**62**]$^{+}$ and [**64**]$^{+}$. Radical localization was confirmed *via* bond length asymmetry in the solid-state structure of the oxidized Pd complexes, and rR in solution exhibited both phenoxyl and phenolate bands. The localized electronic structure determined for Pd contrasted the delocalized electronic structure for Ni and Pt, highlighting that a change in central metal ion can have a substantial impact on the electronic coupling of the two redox-active phenolates. The influence of the central metal ion on the electronic coupling in these oxidized Group 10 salen complexes was also evident in the IVCT bands (Fig. 19). The energy of the intense NIR transition is dependent on the relative energies of the donor and acceptor orbitals, in this case the βHOMO → βLUMO transition predicted by TD-DFT calculations (Fig. 19, inset). The βHOMO is ligand-based, and thus little variation in this orbital occurs across the three oxidized complexes. However, the energy of the βLUMO is dependent on the interaction of the metal d_{xz} orbital with the appropriate ligand orbital. Greater overlap raises the energy of the βLUMO (as this is an antibonding combination) resulting in a blue shift in the IVCT band. Relativistic effects in combination with effective nuclear charge increases the energy of the valence d-orbitals in the order Pd < Ni < Pt, and the energies of the IVCT bands reflect this result [128,162,163]. In addition, the limited overlap between the Pd d_{xz} orbital and the appropriate ligand MO leads to localization of the ligand radical and Class II/III character, as opposed to the Class III character assigned to the oxidized Ni and Pt derivatives.

Final version published in: Coordination Chemistry Reviews 352, 67-82, 2017.
https://doi.org/10.1016/j.ccr.2017.08.019

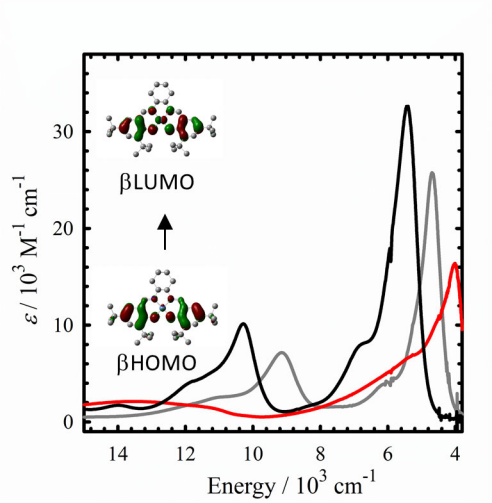

Figure 19. Absorption spectra in the NIR region of [**63**]$^+$ (black), [**17**]$^+$ (grey), and [**64**]$^+$ (red). Inset: Orbitals involved in the TD-DFT calculated NIR transition for [**17**]$^+$.

As previously described for the Ni complex with a propyl backbone (**21**), the Pd and Pt analogues (**65-66**) incorporating the propyl backbone exhibit slightly reduced IVCT band intensities, likely reflecting the increased distortion at the metal center and reduced coupling of the redox-active phenolate moieties [134].

Storr and co-workers recently investigated the electronic structures of oxidized U(VI) salophen complexes (**67-69**) [59]. Oxidation afforded localized U(VI)-phenoxyl radical species, with a small amount of participation of the phenylenediamine backbone in the SOMO. Interestingly, phenoxyl character in the SOMO increased with the electron-donating ability of the *para*-phenolate substituent (NMe_2 > OMe > tBu). Broad and weak NIR bands for [**67**]$^+$ (11,000 cm^{-1}) and [**68**]$^+$ (12,500 cm^{-1}) and more intense bands for [**69**]$^+$ (17,500 cm^{-1} and 18,500 cm^{-1}) supported the assignment as Class II systems.

7. Other Ligands

Final version published in: Coordination Chemistry Reviews 352, 67-82, 2017.
https://doi.org/10.1016/j.ccr.2017.08.019

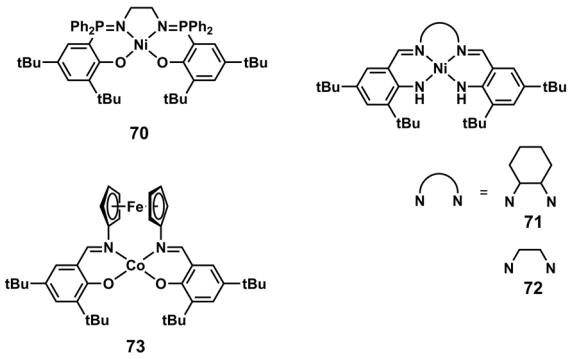

Figure 20. Salen ligand derivatives studied by various groups.

A large number of structurally modified salen ligands have been reported, and here we have chosen to highlight examples which display interesting electronic structure properties (Fig. 20). Auffrant and co-workers presented an example of a tetracoordinate Ni(II) complex containing a phosphasalen ligand, where the imine moiety is substituted for an iminophosphorane (P=N) [164]. One-electron oxidation of this Ni(II) phosphasalen **70** resulted in a rare 4-coordinate high-valent Ni(III) species [165-168]. This contrasts with the exclusive ligand radical formation observed with oxidized Ni(II) salen complexes in the absence of coordinating ligands, *i.e.* **17** or **21**, likely due to the decreased electron density at the phenol rings as a result of the electron-withdrawing phosphorene substituent [164].

Thomas and co-workers have investigated the electronic structures of Ni(II) complexes containing the tetradentate anilinosalen (**71**-**72**) ligand scaffold [169]. Upon oxidation, stable anilino radicals are formed and isolated in the solid state. The oxidized complexes $[\mathbf{71}]^+$ and $[\mathbf{72}]^+$ exhibit intense low energy transitions at *ca*. 6,400 cm^{-1} (above 25,000 M^{-1} cm^{-1}) and were assigned as Class III mixed-valence systems.

Finally, a recent report by Diaconescu and Shepard of a tetrahedral Co(II) salen complex with a ferrocene-containing backbone (**73**) presents an interesting example of the incorporation of a

redox-active backbone unit into a salen-type ligand system [170,171]. **73** was determined to undergo two ligand-centered oxidations when compared to the Zn analogue, with catalytic activity for the hydroalkoxylation of styrenes.

8. Outlook

This review highlights selected foundational work and recent advances in the field of oxidized metal salen complexes. It is clear that the electronic structure of these complexes are sensitive to a variety of factors, including, central metal ion, ligand substitution pattern, solvent and exogenous ligands. We hope to have familiarized the reader not only with the field of oxidized metal salen complexes, but also the techniques used to study this fascinating class of complexes. The electronic structures of oxidized metal systems may be applicable to other non-innocent ligand systems, and we expect that the spectroscopic signatures detailed herein will be useful for the characterization of intermediate species in catalytic systems. There exists a large space for innovation in the field, specifically in the area of reactivities of oxidized metal salen complexes and we look forward to the many breakthroughs to come.

Acknowledgments

The authors would like to thank Prof. Hiroshi Fujii and Prof. Fabrice Thomas for the data presented in Figures 4 and 7. R.M.C. thanks NSERC for a postgraduate fellowship, as well as Mitacs Canada for a Globalink Travel Award. T.S. acknowledges an NSERC Discovery Grant and many collaborators in the field.

References

[1] P.J. Chirik, Inorg. Chem., 50 (2011) 9737-9740.

[2] P.J. Chirik, K. Wieghardt, Science, 327 (2010) 794-795.

[3] V.K.K. Praneeth, M.R. Ringenberg, T.R. Ward, Angew. Chem. Int. Ed., 51 (2012) 10228-10234.

[4] O.R. Luca, R.H. Crabtree, Chemical Society Reviews, 42 (2013) 1440-1459.

[5] W. Kaim, Eur. J. Inorg. Chem., 2012 (2012) 343-348.

[6] V. Lyaskovskyy, B. de Bruin, ACS Catalysis, 2 (2012) 270-279.

[7] J. Stubbe, W.A. van der Donk, Chem. Rev., 98 (1998) 705-762.

[8] I. Pujols-Ayala, B.A. Barry, Biochimica et Biophysica Acta (BBA) - Bioenergetics, 1655 (2004) 205-216.

[9] B.A. Barry, G.T. Babcock, Proc. Natl. Acad. Sci. U. S. A., 84 (1987) 7099-7103.

[10] M.S. Rogers, D.M. Dooley, Curr. Opin. Chem. Biol., 7 (2003) 189-196.

[11] L.D. Slep, F. Neese, Angew. Chem. Int. Ed., 42 (2003) 2942-2945.

[12] M.M. Whittaker, P.J. Kersten, N. Nakamura, J. Sanders-Loehr, E.S. Schweizer, J.W. Whittaker, J. Biol. Chem., 271 (1996) 681-687.

[13] J.W. Whittaker, Chem. Rev., 103 (2003) 2347-2364.

[14] M.M. Whittaker, V.L. DeVito, S.A. Asher, J.W. Whittaker, J. Biol. Chem., 264 (1989) 7104-7106.

[15] M.M. Whittaker, J.W. Whittaker, J. Biol. Chem., 265 (1990) 9610-9613.

[16] L. Que, W.B. Tolman, Nature, 455 (2008) 333-340.

[17] W. Nam, Acc. Chem. Res., 40 (2007) 465-465.

[18] G.F. Swiegers, J. Chen, P. Wagner, Bioinspired Catalysis, in: Bioinspiration and Biomimicry in Chemistry, John Wiley & Sons, Inc., 2012, pp. 165-208.

[19] Y. Wang, J.L. DuBois, B. Hedman, K.O. Hodgson, T.D.P. Stack, Science, 279 (1998) 537-540.

[20] M.S. Chen, M.C. White, Science, 318 (2007) 783-787.

[21] E.V. Kudrik, P. Afanasiev, L.X. Alvarez, P. Dubourdeaux, M. Clémancey, J.-M. Latour, G. Blondin, D. Bouchu, F. Albrieux, S.E. Nefedov, A.B. Sorokin, Nat Chem, 4 (2012) 1024-1029.

[22] E.M. McGarrigle, D.G. Gilheany, Chem. Rev., 105 (2005) 1563-1602.

[23] L. Canali, D. C. Sherrington, Chemical Society Reviews, 28 (1999) 85-93.

[24] D.J. Darensbourg, Chem. Rev., 107 (2007) 2388-2410.

[25] R. Irie, K. Noda, Y. Ito, N. Matsumoto, T. Katsuki, Tetrahedron Lett., 31 (1990) 7345-7348.

[26] E.N. Jacobsen, W. Zhang, A.R. Muci, J.R. Ecker, L. Deng, J. Am. Chem. Soc., 113 (1991) 7063-7064.

[27] C.T. Lyons, T.D.P. Stack, Coord. Chem. Rev., 257 (2013) 528-540.

[28] P.G. Cozzi, Chemical Society Reviews, 33 (2004) 410-421.

[29] R.M. Clarke, T. Storr, Dalton Trans., 43 (2014) 9380-9391.

[30] R.C. Pratt, T.D.P. Stack, J. Am. Chem. Soc., 125 (2003) 8716-8717.

[31] R.C. Pratt, C.T. Lyons, E.C. Wasinger, T.D.P. Stack, J. Am. Chem. Soc., 134 (2012) 7367-7377.

[32] E. Saint-Aman, S. Menage, J.-L. Pierre, E. Defrancq, G. Gellon, New J. Chem., 22 (1998) 393-394.

[33] F. Thomas, O. Jarjayes, C. Duboc, C. Philouze, E. Saint-Aman, J.-L. Pierre, Dalton Trans., (2004) 2662-2669.

[34] E.J. Campbell, S.T. Nguyen, Tetrahedron Lett., 42 (2001) 1221-1225.

[35] P. Audebert, P. Capdevielle, M. Maumy, New J. Chem., 15 (1991) 235-237.

[36] A. Pasini, E. Bernini, M. Scaglia, G. de Santis, Polyhedron, 15 (1996) 4461-4467.

[37] S.M. Abu-El-Wafa, R.M. Issa, C.A. McAuliffe, Inorg. Chim. Acta, 99 (1985) 103-106.

[38] A. Bottcher, H. Elias, E.G. Jager, H. Langfelderova, M. Mazur, L. Muller, H. Paulus, P. Pelikan, M. Rudolph, M. Valko, Inorg. Chem., 32 (1993) 4131-4138.

[39] C. Freire, B. de Castro, J. Chem. Soc. Dalton Trans., (1998) 1491-1497.

[40] W. Kaim, A. Klein, M. Glöckle, Acc. Chem. Res., 33 (2000) 755-763.

[41] K.D. Demadis, C.M. Hartshorn, T.J. Meyer, Chem. Rev., 101 (2001) 2655-2686.

[42] C. Creutz, H. Taube, J. Am. Chem. Soc., 91 (1969) 3988-3989.

[43] P. Chaudhuri, C.N. Verani, E. Bill, E. Bothe, T. Weyhermüller, K. Wieghardt, J. Am. Chem. Soc., 123 (2001) 2213-2223.

[44] C.C. Lu, E. Bill, T. Weyhermüller, E. Bothe, K. Wieghardt, J. Am. Chem. Soc., 130 (2008) 3181-3197.

[45] M.B. Robin, P. Day, Adv. Inorg. Chem. Radiochem., 10 (1967) 247.

[46] N.S. Hush, Intervalence-Transfer Absorption. Part 2. Theoretical Considerations and Spectroscopic Data, in: Prog. Inorg. Chem., John Wiley & Sons, Inc., 2007, pp. 391-444.

[47] U. Fuerholz, S. Joss, H.B. Buergi, A. Ludi, Inorg. Chem., 24 (1985) 943-948.

[48] D.M. D'Alessandro, F.R. Keene, Chem. Soc. Rev., 35 (2006) 424-440.

[49] M. Parthey, M. Kaupp, Chemical Society Reviews, 43 (2014) 5067-5088.

[50] B.S. Brunschwig, C. Creutz, N. Sutin, Chemical Society Reviews, 31 (2002) 168-184.

[51] J.-P. Launay, Chemical Society Reviews, 30 (2001) 386-397.

[52] V. Balzani, A. Juris, M. Venturi, S. Campagna, S. Serroni, Chem. Rev., 96 (1996) 759-834.

[53] N.G. Connelly, W.E. Geiger, Chem. Rev., 96 (1996) 877-910.

[54] J.B. Flanagan, S. Margel, A.J. Bard, F.C. Anson, J. Am. Chem. Soc., 100 (1978) 4248-4253.

[55] C. Creutz, Mixed Valence Complexes of d5-d6 Metal Centers, in: Prog. Inorg. Chem., John Wiley & Sons, Inc., 2007, pp. 1-73.

[56] K. Kalyanasundaram, M.K. Nazeeruddin, Inorg. Chim. Acta, 226 (1994) 213-230.

[57] M.D. Ward, Chemical Society Reviews, 24 (1995) 121-134.

[58] L. Chiang, A. Kochem, O. Jarjayes, T.J. Dunn, H. Vezin, M. Sakaguchi, T. Ogura, M. Orio, Y. Shimazaki, F. Thomas, T. Storr, Chem. Eur. J., 18 (2012) 14117-14127.

[59] K. Herasymchuk, L. Chiang, C.E. Hayes, M.L. Brown, J.S. Ovens, B.O. Patrick, D.B. Leznoff, T. Storr, Dalton Trans., 45 (2016) 12576-12586.

[60] T. Storr, P. Verma, Y. Shimazaki, E.C. Wasinger, T.D.P. Stack, Chem. Eur. J., 16 (2010) 8980-8983.

[61] Y. Shimazaki, F. Tani, K. Fukui, Y. Naruta, O. Yamauchi, J. Am. Chem. Soc., 125 (2003) 10512-10513.

[62] J.G. Radziszewski, M. Gil, A. Gorski, J. Spanget-Larsen, J. Waluk, B.J. Mróz, J. Chem. Phys., 116 (2002) 5912-5912.

[63] J. Spanget-Larsen, M. Gil, A. Gorski, D.M. Blake, J. Waluk, J.G. Radziszewski, J. Am. Chem. Soc., 123 (2001) 11253-11261.

[64] T. Storr, E.C. Wasinger, R.C. Pratt, T.D.P. Stack, Angew. Chem. Int. Ed., 46 (2007) 5198-5201.

[65] T. Storr, P. Verma, R.C. Pratt, E.C. Wasinger, Y. Shimazaki, T.D.P. Stack, J. Am. Chem. Soc., 130 (2008) 15448-15459.

[66] C.J. Cramer, Essentials of Computational Chemistry: Theories and Models, 2 ed., John Wiley & Sons Ltd, 2004.

[67] D.F. Evans, J. Chem. Soc., (1959) 2003-2005.

[68] D.F. Evans, G.V. Fazakerley, R.F. Phillips, J. Chem. Soc. A, (1971) 1931-1934.

[69] K.K. Krishnan, A.M. Thomas, K.S. Sindhu, G. Anilkumar, Tetrahedron, 72 (2016) 1-16.

[70] T. Katsuki, Adv. Synth. Catal., 344 (2002) 131-147.

[71] T. Katsuki, Synlett, 2003 (2003) 0281-0297.

[72] T.R.J. Achard, L.A. Clutterbuck, M. North, Synlett, 2005 (2005) 1828-1847.

[73] X. Huang, W. Liu, H. Ren, R. Neelamegam, J.M. Hooker, J.T. Groves, J. Am. Chem. Soc., 136 (2014) 6842-6845.

[74] J. Du Bois, J. Hong, E.M. Carreira, M.W. Day, J. Am. Chem. Soc., 118 (1996) 915-916.

[75] J. Du Bois, C.S. Tomooka, J. Hong, E.M. Carreira, Acc. Chem. Res., 30 (1997) 364-372.

[76] J. Du Bois, C.S. Tomooka, J. Hong, E.M. Carreira, J. Am. Chem. Soc., 119 (1997) 3179-3180.

[77] G. Golubkov, Z. Gross, J. Am. Chem. Soc., 127 (2005) 3258-3259.

[78] J. Bendix, J. Am. Chem. Soc., 125 (2003) 13348-13349.

[79] T. Birk, J. Bendix, Inorg. Chem., 42 (2003) 7608-7615.

[80] S.-E. Park, W.J. Song, Y.O. Ryu, M.H. Lim, R. Song, K.M. Kim, W. Nam, J. Inorg. Biochem., 99 (2005) 424-431.

[81] J.P. Collman, L. Zeng, J.I. Brauman, Inorg. Chem., 43 (2004) 2672-2679.

[82] C. Wang, T. Kurahashi, K. Inomata, M. Hada, H. Fujii, Inorg. Chem., 52 (2013) 9557-9566.

[83] H. Jacobsen, L. Cavallo, Organometallics, 25 (2006) 177-183.

[84] M. Sankaralingam, M. Palaniandavar, Dalton Trans., 43 (2014) 538-550.

[85] S. Liao, B. List, Angew. Chem. Int. Ed., 49 (2010) 628-631.

[86] T. Kurahashi, A. Kikuchi, T. Tosha, Y. Shiro, T. Kitagawa, H. Fujii, Inorg. Chem., 47 (2008) 1674-1686.

[87] T. Kurahashi, Y. Kobayashi, S. Nagatomo, T. Tosha, T. Kitagawa, H. Fujii, Inorg. Chem., 44 (2005) 8156-8166.

[88] T. Kurahashi, H. Fujii, J. Am. Chem. Soc., 133 (2011) 8307-8316.

[89] T. Kurahashi, M. Hada, H. Fujii, J. Am. Chem. Soc., 131 (2009) 12394-12405.

[90] S. Aono, M. Nakagaki, T. Kurahashi, H. Fujii, S. Sakaki, J. Chem. Theory Comput., 10 (2014) 1062-1073.

[91] R.M. Clarke, T. Storr, J. Am. Chem. Soc., 138 (2016) 15299-15302.

[92] W.-L. Man, T.-M. Tang, T.-W. Wong, T.-C. Lau, S.-M. Peng, W.-T. Wong, J. Am. Chem. Soc., 126 (2004) 478-479.

[93] W.-L. Man, G. Chen, S.-M. Yiu, L. Shek, W.-Y. Wong, W.-T. Wong, T.-C. Lau, Dalton Trans., 39 (2010) 11163-11170.

[94] W.-L. Man, H.-K. Kwong, W.W.Y. Lam, J. Xiang, T.-W. Wong, W.-H. Lam, W.-T. Wong, S.-M. Peng, T.-C. Lau, Inorg. Chem., 47 (2008) 5936-5944.

[95] S.-M. Yiu, W.W.Y. Lam, C.-M. Ho, T.-C. Lau, J. Am. Chem. Soc., 129 (2007) 803-809.

[96] J. Dimroth, M. Weck, RSC Advances, 5 (2015) 29108-29113.

[97] K. Lang, J. Park, S. Hong, Angew. Chem. Int. Ed., 51 (2012) 1620-1624.

[98] J.D. White, S. Shaw, Org. Lett., 16 (2014) 3880-3883.

[99] J. Park, K. Lang, K.A. Abboud, S. Hong, J. Am. Chem. Soc., 130 (2008) 16484-16485.

[100] X.-B. Lu, L. Shi, Y.-M. Wang, R. Zhang, Y.-J. Zhang, X.-J. Peng, Z.-C. Zhang, B. Li, J. Am. Chem. Soc., 128 (2006) 1664-1674.

[101] N.S. Venkataramanan, G. Kuppuraj, S. Rajagopal, Coord. Chem. Rev., 249 (2005) 1249-1268.

[102] L. Chiang, L.E.N. Allan, J. Alcantara, M.C.P. Wang, T. Storr, M.P. Shaver, Dalton Trans., 43 (2014) 4295-4304.

[103] E.N. Jacobsen, Acc. Chem. Res., 33 (2000) 421-431.

[104] J.M. Ready, E.N. Jacobsen, J. Am. Chem. Soc., 123 (2001) 2687-2688.

[105] M.E. Furrow, S.E. Schaus, E.N. Jacobsen, The Journal of Organic Chemistry, 63 (1998) 6776-6777.

[106] S.E. Schaus, B.D. Brandes, J.F. Larrow, M. Tokunaga, K.B. Hansen, A.E. Gould, M.E. Furrow, E.N. Jacobsen, J. Am. Chem. Soc., 124 (2002) 1307-1315.

[107] L.P.C. Nielsen, C.P. Stevenson, D.G. Blackmond, E.N. Jacobsen, J. Am. Chem. Soc., 126 (2004) 1360-1362.

[108] C.L. Bailey, R.S. Drago, Coord. Chem. Rev., 79 (1987) 321-332.

[109] K. Kervinen, P. Lahtinen, T. Repo, M. Svahn, M. Leskelä, Catal. Today, 75 (2002) 183-188.

[110] K. Kervinen, H. Korpi, M. Leskelä, T. Repo, Journal of Molecular Catalysis A: Chemical, 203 (2003) 9-19.

[111] S.R. Collinson, W. Thielemans, Coord. Chem. Rev., 254 (2010) 1854-1870.

[112] E. Vinck, D.M. Murphy, I.A. Fallis, R.R. Strevens, S. Van Doorslaer, Inorg. Chem., 49 (2010) 2083-2092.

[113] S. Kemper, P. Hrobárik, M. Kaupp, N.E. Schlörer, J. Am. Chem. Soc., 131 (2009) 4172-4173.

[114] D.E. White, E.N. Jacobsen, Tetrahedron: Asymmetry, 14 (2003) 3633-3638.

[115] A. Kochem, H. Kanso, B. Baptiste, H. Arora, C. Philouze, O. Jarjayes, H. Vezin, D. Luneau, M. Orio, F. Thomas, Inorg. Chem., 51 (2012) 10557-10571.

[116] T. Kurahashi, H. Fujii, Inorg. Chem., 52 (2013) 3908-3919.

[117] R.M. Clarke, K. Hazin, J.R. Thompson, D. Savard, K.E. Prosser, T. Storr, Inorg. Chem., 55 (2016) 762-774.

[118] J. Andrez, V. Guidal, R. Scopelliti, J. Pécaut, S. Gambarelli, M. Mazzanti, J. Am. Chem. Soc., (2017).

[119] F. Thomas, Dalton Trans., 45 (2016) 10866-10877.

[120] B. De Castro, C. Freire, Inorg. Chem., 29 (1990) 5113-5119.

[121] I.C. Santos, M. Vilas-Boas, M.F.M. Piedade, C. Freire, M.T. Duarte, B. de Castro, Polyhedron, 19 (2000) 655-664.

[122] W.-H. Leung, E.Y.Y. Chan, E.K.F. Chow, I.D. Williams, S.-M. Peng, J. Chem. Soc. Dalton Trans., (1996) 1229-1236.

[123] O. Rotthaus, F. Thomas, O. Jarjayes, C. Philouze, E. Saint-Aman, J.-L. Pierre, Chem. Eur. J., 12 (2006) 6953-6962.

[124] O. Rotthaus, O. Jarjayes, F. Thomas, C. Philouze, C.P. Del Valle, E. Saint-Aman, J.L. Pierre, Chem. Eur. J., 12 (2006) 2293-2302.

[125] L. Benisvy, R. Kannappan, Y.-F. Song, S. Milikisyants, M. Huber, I. Mutikainen, U. Turpeinen, P. Gamez, L. Bernasconi, E.J. Baerends, F. Hartl, J. Reedijk, Eur. J. Inorg. Chem., 2007 (2007) 637-642.

[126] M. Orio, O. Jarjayes, H. Kanso, C. Philouze, F. Neese, F. Thomas, Angew. Chem. Int. Ed., 49 (2010) 4989-4992.

[127] L. Chiang, K. Herasymchuk, F. Thomas, T. Storr, Inorg. Chem., 54 (2015) 5970-5980.

[128] Y. Shimazaki, T.D.P. Stack, T. Storr, Inorg. Chem., 48 (2009) 8383-8392.

[129] M. Malik, R. Wysokiński, W. Zierkiewicz, K. Helios, D. Michalska, J. Phys. Chem. A, 118 (2014) 6922-6934.

[130] P. Dev, S. Agrawal, N.J. English, J. Phys. Chem. A, 117 (2013) 2114-2124.

[131] L. Chiang, R.M. Clarke, K. Herasymchuk, M. Sutherland, K.E. Prosser, Y. Shimazaki, T. Storr, Eur. J. Inorg. Chem., 2016 (2016) 49-55.

[132] T.J. Dunn, M.I. Webb, K. Hazin, P. Verma, E.C. Wasinger, Y. Shimazaki, T. Storr, Dalton Trans., 42 (2013) 3950-3956.

[133] M. Kawai, T. Yamaguchi, S. Masaoka, F. Tani, T. Kohzuma, L. Chiang, T. Storr, K. Mieda, T. Ogura, R.K. Szilagyi, Y. Shimazaki, Inorg. Chem., 53 (2014) 10195-10202.

[134] Y. Shimazaki, N. Arai, T.J. Dunn, T. Yajima, F. Tani, C.F. Ramogida, T. Storr, Dalton Trans., 40 (2011) 2469-2479.

[135] L. Lecarme, L. Chiang, C. Philouze, O. Jarjayes, T. Storr, F. Thomas, Eur. J. Inorg. Chem., 2014 (2014) 3479-3487.

[136] O. Rotthaus, O. Jarjayes, C. Perez Del Valle, C. Philouze, F. Thomas, Chem. Commun., (2007) 4462-4464.

[137] O. Rotthaus, O. Jarjayes, C. Philouze, C.P. Del Valle, F. Thomas, Dalton Trans., (2009) 1792-1800.

[138] D. de Bellefeuille, M.S. Askari, B. Lassalle-Kaiser, Y. Journaux, A. Aukauloo, M. Orio, F. Thomas, X. Ottenwaelder, Inorg. Chem., 51 (2012) 12796-12804.

[139] A. Kochem, M. Orio, O. Jarjayes, F. Neese, F. Thomas, Chem. Commun., 46 (2010) 6765-6767.

[140] E. Bill, J. Müller, T. Weyhermüller, K. Wieghardt, Inorg. Chem., 38 (1999) 5795-5802.

[141] P. Chaudhuri, M. Hess, J. Müller, K. Hildenbrand, E. Bill, T. Weyhermüller, K. Wieghardt, J. Am. Chem. Soc., 121 (1999) 9599-9610.

[142] F. Thomas, Eur. J. Inorg. Chem., 2007 (2007) 2379-2404.

[143] Y. Wang, T.D.P. Stack, J. Am. Chem. Soc., 118 (1996) 13097-13098.

[144] R.C. Pratt, T.D.P. Stack, Inorg. Chem., 44 (2005) 2367-2375.

[145] P. Verma, R.C. Pratt, T. Storr, E.C. Wasinger, T.D.P. Stack, Proc. Natl. Acad. Sci. U. S. A., 108 (2011) 18600-18605.

[146] C.G. Pierpont, Coord. Chem. Rev., 216–217 (2001) 99-125.

[147] D.M. Adams, L. Noodleman, D.N. Hendrickson, Inorg. Chem., 36 (1997) 3966-3984.

[148] D.N. Hendrickson, C.G. Pierpont, Valence Tautomeric Transition Metal Complexes, in: Spin Crossover in Transition Metal Compounds II, Springer Berlin Heidelberg, Berlin, Heidelberg, 2004, pp. 63-95.

[149] J. Rall, M. Wanner, M. Albrecht, F.M. Hornung, W. Kaim, Chem. Eur. J., 5 (1999) 2802-2809.

[150] G. Speier, Z. Tyeklár, P. Tóth, E. Speier, S. Tisza, A. Rockenbauer, A.M. Whalen, N. Alkire, C.G. Pierpont, Inorg. Chem., 40 (2001) 5653-5659.

[151] D. Rokhsana, D.M. Dooley, R.K. Szilagyi, J. Am. Chem. Soc., 128 (2006) 15550-15551.

[152] A. Kochem, O. Jarjayes, B. Baptiste, C. Philouze, H. Vezin, K. Tsukidate, F. Tani, M. Orio, Y. Shimazaki, F. Thomas, Chem. Eur. J., 18 (2012) 1068-1072.

[153] D. de Bellefeuille, M. Orio, A.-L. Barra, A. Aukauloo, Y. Journaux, C. Philouze, X. Ottenwaelder, F. Thomas, Inorg. Chem., 54 (2015) 9013-9026.

[154] K. Asami, A. Takashina, M. Kobayashi, S. Iwatsuki, T. Yajima, A. Kochem, M. van Gastel, F. Tani, T. Kohzuma, F. Thomas, Y. Shimazaki, Dalton Trans., 43 (2014) 2283-2293.

[155] K.M. Kadish, M. Lin, E.V. Caemelbecke, G. De Stefano, C.J. Medforth, D.J. Nurco, N.Y. Nelson, B. Krattinger, C.M. Muzzi, L. Jaquinod, Y. Xu, D.C. Shyr, K.M. Smith, J.A. Shelnutt, Inorg. Chem., 41 (2002) 6673-6687.

[156] K. Butsch, T. Günther, A. Klein, K. Stirnat, A. Berkessel, J. Neudörfl, Inorg. Chim. Acta, 394 (2013) 237-246.

[157] K. Asami, K. Tsukidate, S. Iwatsuki, F. Tani, S. Karasawa, L. Chiang, T. Storr, F. Thomas, Y. Shimazaki, Inorg. Chem., 51 (2012) 12450-12461.

[158] A. Soroceanu, M. Cazacu, S. Shova, C. Turta, J. Kožíšek, M. Gall, M. Breza, P. Rapta, T.C.O. Mac Leod, A.J.L. Pombeiro, J. Telser, A.A. Dobrov, V.B. Arion, Eur. J. Inorg. Chem., 2013 (2013) 1458-1474.

[159] M. Franks, A. Gadzhieva, L. Ghandhi, D. Murrell, A.J. Blake, E.S. Davies, W. Lewis, F. Moro, J. McMaster, M. Schröder, Inorg. Chem., 52 (2013) 660-670.

[160] L. Benisvy, E. Bill, A.J. Blake, D. Collison, E.S. Davies, C.D. Garner, G. McArdle, E.J.L. McInnes, J. McMaster, S.H.K. Ross, C. Wilson, Dalton Trans., (2006) 258-267.

[161] Y. Shimazaki, T. Yajima, F. Tani, S. Karasawa, K. Fukui, Y. Naruta, O. Yamauchi, J. Am. Chem. Soc., 129 (2007) 2559-2568.

[162] K. Ray, T. Petrenko, K. Wieghardt, F. Neese, Dalton Trans., (2007) 1552-1566.

[163] K. Ray, T. Weyhermüller, F. Neese, K. Wieghardt, Inorg. Chem., 44 (2005) 5345-5360.

[164] T.-P.-A. Cao, G. Nocton, L. Ricard, X.F. Le Goff, A. Auffrant, Angew. Chem. Int. Ed., 53 (2014) 1368-1372.

[165] T.J. Collins, T.R. Nichols, E.S. Uffelman, J. Am. Chem. Soc., 113 (1991) 4708-4709.

[166] V.M. Iluc, A.J.M. Miller, J.S. Anderson, M.J. Monreal, M.P. Mehn, G.L. Hillhouse, J. Am. Chem. Soc., 133 (2011) 13055-13063.

[167] P.J. Alonso, A.B. Arauzo, M.A. García-Monforte, A. Martín, B. Menjón, C. Rillo, M. Tomás, Chem. Eur. J., 15 (2009) 11020-11030.

[168] M.I. Lipschutz, X. Yang, R. Chatterjee, T.D. Tilley, J. Am. Chem. Soc., 135 (2013) 15298-15301.

[169] A. Kochem, G. Gellon, N. Leconte, B. Baptiste, C. Philouze, O. Jarjayes, M. Orio, F. Thomas, Chem. Eur. J., 19 (2013) 16707-16721.

[170] S.M. Shepard, P.L. Diaconescu, Organometallics, 35 (2016) 2446-2453.

[171] C. Bejger, Y.-H. Tian, B.J. Barker, K.S. Boland, B.L. Scott, E.R. Batista, S.A. Kozimor, J.L. Sessler, Dalton Trans., 42 (2013) 6716-6719.